Sedimentary basin controls on orogenic gold deposits: New constraints from U-Pb detrital zircon and Re-Os sulphide geochronology, Lynn Lake greenstone belt, Canada

Lawley, C.J.M.[1†], Yang, X.M.[2], Selby, D.[3,4], Davis, W.[1], Zhang, S.[5], Petts, D.C.[1] and Jackson, S.E.[1]

[1]Natural Resources Canada, Geological Survey of Canada, 601 Booth Street, Ottawa, Ontario, K1A 0E8, Canada
[2]Manitoba Geological Survey, 360-1395 Ellice Avenue, Winnipeg, Manitoba, R3G 3P2, Canada
[3]Department of Earth Sciences, Durham University, Science Labs, Lower Mountjoy, South Rd, Durham, DH1 3LE, UK
[4]State Key Laboratory of Geological Processes and Mineral Resources, School of Earth Resources, China University of Geosciences, Wuhan, 430074, Hubei, China
[5]Department of Earth Sciences, Carleton University, Room 2115 Herzberg Laboratories, 1125 Colonel By Drive, Ottawa, Ontario K1S 5B6, Canada

[†]Corresponding author: christopher.lawley@canada.ca

Keywords: Lynn Lake, Trans-Hudson, conglomerate, basins, orogenic gold, Timiskaming

Abstract

Sedimentary basins that open and close during the last stages of mountain building represent an important exploration criterion for orogenic gold deposits. However, the genetic and/or preservation controls of these synorogenic, or "Timiskaming-type", sedimentary basins and their controlling fault systems on orogenic gold deposits remain unclear. Herein we address that knowledge gap and report new U-Pb detrital zircon and Re-Os sulphide (arsenopyrite and pyrite) geochronology and sulphide Pb isotope results for the Paleoproterozoic Lynn Lake greenstone belt (LLGB), Manitoba, Canada. The youngest detrital zircon from all six meta-conglomerate and -psammite samples of the synorogenic Sickle Group, and previously reported U-Pb zircon ages for post-Sickle Group intrusions, are used to constrain its depositional timing from 1836 ± 15 to 1831 ± 4 Ma. Replicate analyses of one highly-radiogenic arsenopyrite sample from an auriferous vein at the MacLellan gold deposit yield a weighted average Re-Os

model age of 1824 ± 12 Ma, which is identical to previously published in situ U-Pb xenotime ages at the same deposit (1827 ± 8 Ma). Each of these hydrothermal ages demonstrate that early-stage auriferous veins immediately post-date deposition of the Sickle Group and most likely occurred prior to peak metamorphism (1814–1801 Ma). This sequence of events is very similar to the Abitibi greenstone belt, suggesting that a synorogenic phase of extension and rapid burial of auriferous veins by Timiskaming-type Sickle Group sediments may have played an important genetic and/or preservation control on early-stage gold mineralization in the LLGB. However, unlike the Abitibi greenstone belt, none of the known gold deposits within the LLGB are hosted within the Sickle Group. Younger Re-Os model arsenopyrite ages at 1782 ± 16 Ma from the MacLellan gold deposit also post-date synorogenic sedimentary basins by ca. 50 Myr. These late-stage auriferous veins are unrelated to the synorogenic extensional phase and more likely reflect repeated fluid focusing along reactivated structures during a post-peak metamorphic phase of hydrothermal activity. The multi-stage hydrothermal history of orogenic gold deposits in the LLGB also provides a possible explanation for the mixture of depleted mantle-like and highly radiogenic fluid components that are inferred from age-corrected sulphide Pb isotope compositions ($\mu_{1.8\ Ga}$ = 8.9–10.6). Reworked cratonic margins and their associated greenstone belts thus represent favourable depositional settings for auriferous fluids at multiple stages throughout the lifespan of an orogen.

1 Introduction

Mountain systems are enormous features of Earth's continental crust that stretch along strike for 1000s of kilometres and take 10s to 100s of millions of years to build. The process of mountain building is often referred to as orogenesis and may involve accretionary stages during the subduction of oceanic lithosphere and collisional stages after the ocean floor between two continental blocks has been completely subducted (Cawood et al., 2009; Wilson, 1966). Orogenic gold deposits are somewhat unique relative to other ore systems because they can form at various stages of orogenesis (e.g., accretionary and collisional) and are hosted by multiple rock types of all geological ages (Goldfarb et al., 2001; Groves et al., 1998; Kerrich and Wyman, 1990). Most authors attribute gold transport in these settings to metamorphic fluids

based on the broad "syn" orogenic timing and isotopic signature (C-O-S isotope) of the auriferous veins. However, recent advances in geochronology have demonstrated that many orogenic gold districts are characterized by multiple, overprinting hydrothermal events that in detail may pre- and/or post-date the peak metamorphic timing of their host rocks (Arne et al., 2001; Lawley et al., 2015, 2013; Le Mignot et al., 2017; Morelli et al., 2005; Rasmussen et al., 2006). The pre- and post-metamorphic timing of auriferous veins and multi-stage hydrothermal history of these orogenic gold deposits is inconsistent with gold-bearing fluids of local metamorphic origin. Resolving the complete source-to-ore pathways of these gold ore systems and their drivers within an evolving orogen thus require precise age constraints for the timing of gold deposition, metamorphism, and magmatism during each orogenic stage.

Many orogenic gold deposits also share a close spatial and temporal relationship with sedimentary basins that open and close during the last stages of orogenesis (Barley et al., 1989; Bleeker, 2012; Cameron, 1993; Krapež and Barley, 2008; Poulsen et al., 1992). In the Neoarchean Abitibi greenstone belt, these synorogenic sedimentary rocks are concentrated along the two main auriferous faults and are referred to as Timiskaming-type basins (Bleeker, 2015, 2012; Cameron, 1993; Poulsen et al., 1992). Detailed structural and geochronology studies in the Timmins area suggests that rapid burial of auriferous veins following a synorogenic phase of extension may have played an important genetic and preservation control on orogenic gold deposits (Bleeker, 2015, 2012). However, precise geochronology constraints for the timing of sedimentation are required to test whether Timiskaming-type sedimentary basins can be used as an exploration vector in other gold districts.

Herein we address those knowledge gaps and report new U-Pb detrital zircon and Re-Os sulphide (arsenopyrite and pyrite) geochronology results for the Paleoproterozoic Lynn Lake greenstone belt. These ages, combined with previously reported metamorphic and igneous age constraints, provide a more complete picture of the various stages of accretionary and collisional orogenesis within the southwestern Tran-Hudson Orogen (THO). We demonstrate that early-stage auriferous veins immediately post-date a synorogenic phase of extension and sedimentation, but occurred ca. 10 Myr prior to peak amphibolite facies metamorphism. New ages further demonstrate that late-stage arsenopyrite post-date peak metamorphism

by ca. 30 Myr. The implications of this new temporal framework to orogenic gold deposit genesis in the LLGB are discussed below.

2 Regional geology

The THO is a Paleoproterozoic (1.9–1.8 Ga) collision zone that formed after the closure of the Manikewan ocean (Corrigan et al., 2009; Hoffman, 1988; Stauffer, 1984). In Manitoba and Saskatchewan, continental collision involved three main cratonic blocks (i.e., Superior, Hearne, and Sask cratons; Fig. 1)(Ansdell, 2005; Ashton et al., 1999; Bickford et al., 1990; Hoffman, 1988; Lewry et al., 1994). Multiple Paleoproterozoic granite-greenstone belts (e.g., Flin Flon, Glennie, La Ronge, and Lynn Lake), which separate these three cratonic blocks, comprise the Reindeer Zone and represent some of the only remnants of what was likely a vast (1000s of km) intervening ocean basin (Ansdell, 2005; Stauffer, 1984; Symons and Harris, 2005). The oldest arc fragments from all three granite-greenstone belts suggests that the Manikewan ocean closure likely started at ≤ 1.92 Ga (Ansdell, 2005; Corrigan et al., 2009; Maxeiner and Rayner, 2011).

The Lynn Lake greenstone belt (LLGB) represents one example of these Paleoproterozoic arc-related ultramafic to felsic rock assemblages hosted within the interior, or internides, of the THO (Fig. 1–3)(Baldwin et al., 1987; Bateman, 1942; Gilbert et al., 1980; Milligan, 1960; Syme, 1985). To the west, the LLGB is mostly correlative with the La Ronge greenstone belt in Saskatchewan (Fig. 1)(Maxeiner and Demmans, 2000). To the south, the LLGB is separated from the broadly coeval Flin Flon greenstone belt by the Paleoproterozoic Kisseynew basin (Fig. 1)(Ansdell and Norman, 1995; Machado et al., 1999; White, 2005; Zwanzig, 1997, 1999). All three greenstone belts and the intervening Kisseynew sedimentary basin have been deformed and metamorphosed at amphibolite facies during multiple stages of arc accretion and continent-continent collisions as part of the THO (Ansdell, 2005; Bickford et al., 1990; Corrigan et al., 2009, 2005; Lewry et al., 1994; Lewry, 1981).

In the LLGB, the oldest mafic to felsic metavolcanic rock package and its associated metasedimentary successions (e.g., banded iron formation, BIF; conglomerate; greywacke; and

volcaniclastic rocks) comprise the Wasekwan Group (1.91–1.85 Ga; Fig. 2–3)(Baldwin et al., 1987; Beaumont-Smith et al., 2006; Beaumont-Smith and Böhm, 2002; Gilbert et al., 1980; Milligan, 1960; Syme, 1985). Multiple stages of felsic volcanism (1892–1886 and 1856–1842 Ma)(Beaumont-Smith and Böhm, 2003, 2002), coupled with a wide range of mafic volcanic rock compositions, each pointing to a unique geodynamic setting, suggest that the Wasekwan Group consists of multiple terranes that were later structurally juxtaposed (Beaumont-Smith, 2008; Beaumont-Smith and Böhm, 2003, 2002; Zwanzig et al., 1999). Overall, mafic volcanic rocks are dominated by arc-like trace element signatures with mafic volcanic rock compositions of mixed tholeiitic to calc-alkaline character (Beaumont-Smith, 2008; Zwanzig et al., 1999). Isotopic evidence (Sm-Nd) suggests that some of these mafic volcanic rocks interacted with older, and currently unexposed, continental crust, consistent with volcanism along a rifted continental-margin (Beaumont-Smith and Böhm, 2003, 2002). Lesser mafic volcanic rocks with mid-ocean ridge (MORB)- to enriched ocean island basalt (OIB)-like trace element signatures possibly formed in an intra-oceanic setting and may be unrelated to arc volcanism (Glendenning et al., 2014). The isotopic, geochemical, and age differences (e.g., ca. 1.91 versus 1.85 Ga) between the different mafic to felsic volcanic rock packages have been used to separate the LLGB into at least three sub-domains: (1) Northern; (2) Southern; and (3) Fox (Beaumont-Smith and Böhm, 2003; Zwanzig et al., 1999). However, mapping these individual rock packages within the multiply deformed and metamorphosed LLGB remains a significant challenge (Beaumont-Smith and Böhm, 2003; Glendenning et al., 2014; Zwanzig et al., 1999). In Saskatchewan, a succession of mafic tectonite, harzburgite, pillow basalt, pelite, and iron formation, referred to as the Lawrence Point lithotectonic assemblage, has been interpreted as a dismembered supra-subduction zone ophiolite (Maxeiner et al., 2005); it was assumed to be ca. 1.9 Ga and forms the southern component of the La Ronge Domain, along strike of the southern Lynn Lake belt.

The timing of structural imbrication for each of the LLGB sub-domains is constrained by the age of mafic, intermediate, and felsic plutons comprising the 1.89–1.87 Ga Pool Lake suite (Turek et al., 2000). These intrusions stitch mafic volcanic rock packages and each of the LLGB sub-domains (Beaumont-Smith and Böhm, 2003, 2002; Zwanzig et al., 1999), suggesting that at least some of the disparate volcanic

environments were amalgamated prior to ca. 1.87 Ga. Gabbroic rocks that host the Lynn Lake Ni mine are coeval with the youngest examples of the Pool Lake igneous suite (1871 ± 2 and 1870 ± 6 Ma)(Turek et al., 2000). The amalgamated LLGB was then intruded by a second suite of ca. 1.85 Ga intermediate to felsic intrusions (Beaumont-Smith et al., 2006; Beaumont-Smith and Böhm, 2003, 2002). The nominally younger ages of these intrusions have special regional geological significance because they are coeval with the Wathaman-Chipewyan batholith, which stiches the La Ronge-LLGB segment of the THO to the southern Hearne cratonic margin (Fumerton et al., 1984; Meyer et al., 1992). Smaller granitic to intermediate intrusions and dykes of similar age within the LLGB gold deposit stratigraphy may thus mark its final transition from an oceanic arc-environment to a continental setting (Yang and Lawley, 2018). However, in Saskatchewan, Wathaman-aged plutons such as the 1.859 Ga Butler Island diorite (Corrigan et al., 2001) intruding the Lawrence Point lithotectonic assemblage of the La Ronge Domain are instead interpreted as evidence for ongoing intraoceanic subduction (Maxeiner et al., 2005). Similar 1.86–1.85 Ga rhyodacite intrusions in the LLGB are possibly interpreted as the equivalents of this younger juvenile arc (Beaumont-Smith and Böhm, 2003). Because the Pool Lake igneous suite (1.89–1.87 Ga) contains similar rock types, the spatial distribution of the Wathaman-aged intrusions (ca. 1.85 Ga) and younger, arc-related volcanic rock packages within the LLGB remains poorly understood. Hereafter the ca. 1.85 Ga intrusions are referred to as the Burge Lake igneous suite (Beaumont-Smith et al., 2006) and are similar in timing to the "successor-arc" plutons elsewhere in the Reindeer Zone (Syme, 1988).

Younger meta-sedimentary successions (i.e., cobble to pebble conglomerate, psammite, arkose) comprising the Sickle Group unconformably overly the 1.90–1.87 Ga Wasekwan Group and 1.89–1.87 Ga Pool Lake igneous suite (Fig. 4). Late tonalitic to pegmatitic dykes and intrusions are demonstrated to cut the Sickle Group in places. The oldest examples of these inferred post-Sickle Group intrusions, such as the Fox Mine tonalite, provide a minimum depositional U-Pb zircon crystallization age at 1831 ± 4 Ma (Beaumont-Smith and Böhm, 2004, 2003, 2002; Turek et al., 2000). A syn-deformational tonalite dyke that cuts meta-sedimentary rocks comprising the folded Wasekwan Group provides a near identical U-Pb zircon age at 1829 ± 2 Ma, suggesting that burial of the Sickle Group was rapidly followed by folding and faulting

(Beaumont-Smith and Böhm, 2003). The maximum depositional age of the Sickle Group is the focus of the current study and is discussed below. Rare exposures of turbidite-like meta-greywacke and -mudstone comprising the Burntwood Group (i.e., Kisseynew basin) are folded and intercalated with the Sickle Group in the southwest corner of the LLGB (Fig. 2). The Burntwood Group is the main sedimentary rock package comprising the large 1.86–1.83 Ga Kisseynew basin (Fig. 2–3)(Ansdell et al., 1995; Machado et al., 1999; White, 2005; Zwanzig, 1999).

Multiple deformation events have been identified in the LLGB with the earliest recognized deformation phase corresponding to the faulted contacts between the disparate volcanic rocks packages of the Wasekwan Group (Anderson and Böhm, 2001; Beaumont-Smith and Böhm, 2002; Ma and Beaumont-Smith, 2001; Park and Lentz, 2002). However, the main deformation phase (D_2) corresponds to isoclinal folds and a penetrative W-trending S_2 fabric that can be traced for over 100 km across the LLGB (Fig. 2). All of the known gold deposits are controlled by the D_2 stage of deformation (Beaumont-Smith and Böhm, 2003). Re-folded map patterns at district scale and detailed field-based studies suggest that multiple fabric and fold generations re-work and overprint S_2 (Anderson and Böhm, 2001; Beaumont-Smith and Böhm, 2004, 2003; Hastie et al., 2018; Park and Lentz, 2002; Samson and Gagnon, 1995; Samson et al., 1999). These younger and overprinting deformation phases (D_3, D_4, D_5, and D_6) are important because, in some cases, they appear to exert a control on the gold-bearing veins and their volcanic host rock stratigraphy, which are both of interest to on-going mineral exploration in the district (discussed below).

Peak metamorphism and the main stage of deformation post-date all rock types of the LLGB and the Kisseynew basin, except perhaps for some small and late-stage tonalitic (1819 ± 1 Ma) and pegmatitic (1815 ± 3 Ma) dykes (Beaumont-Smith and Böhm, 2004, 2003, 2002). These late-stage dykes constrain the timing of D_2 to between 1819–1815 Ma. The earliest timing for regional metamorphism in the LLGB is constrained between 1814–1801 Ma, based on U-Pb dating of suspected metamorphic zircons (1814 ± 1 Ma and 1801 ± 15 Ma) hosted within the older igneous plutons and dykes (Beaumont-Smith and Böhm, 2003, 2002). Some of these older igneous plutons were associated with an earlier and cryptic phase of contact metamorphism that is overprinted by the regional event linked to D_2. Late-stage tonalitic and

pegmatitic dykes that are syn- to post-date D_2 host even younger metamorphic zircon and titanite (1783 ± 3 Ma; 1766 ± 15 Ma; 1758 ± 8 Ma), suggesting that high-grade metamorphic mineral growth may have continued episodically until at least ca. 1.76 Ga (Beaumont-Smith and Böhm, 2003, 2002). Pegmatite dykes with crystallization and/or metamorphic ages at 1.78–1.77 Ga are interpreted to by syn-D_3; whereas deformed tonalite dykes that yield U-Pb zircon age at 1758 ± 8 Ma correspond to D_4 (Beaumont-Smith and Böhm, 2002). This broad ca. 56 Myr interval is consistent with metamorphic ages peripheral to the LLGB, which define peak metamorphism at 1.81–1.80 Ga and a cryptic secondary metamorphic event and/or thermal pulse at 1.79–1.78 Ga (Couëslan et al., 2013; Schneider et al., 2007). Evidence for earlier regional metamorphic ages have been reported elsewhere in the Reindeer Zone (e.g., ca. 1.83 Ga) and north of Lynn Lake, although their significance in the LLGB remains unclear (Ansdell and Norman, 1995; Couëslan et al., 2013; Machado et al., 2011, 1999). Biotite cooling ages (K-Ar and ^{40}Ar-^{39}Ar) suggest that temperatures in the LLGB were below 400–300°C after ca. 1.77 Ga (Lowdon et al., 1963; Moore et al., 1960; O'Connor et al., 2019; Turek, 1967).

The peak metamorphic assemblage within the meta-volcanic host rocks of the Fox mine comprise biotite-garnet-sillimanite-cordierite-cummingtonite, suggesting temperatures in excess of 550°C at moderate pressure (3 kbar) in the westernmost LLGB (Elliott-Meadows et al., 2000). Preliminary garnet-biotite thermometry results at the MacLellan deposit support these temperature estimates (535–560°C) (O'Connor et al., 2019) and are consistent with middle amphibolite facies metamorphism across the LLGB. Despite the broadly coeval timing of metamorphism, metamorphic temperatures in the Kisseynew basin immediately south of the LLGB were considerably higher (upper amphibolite facies) based on extensive development of garnet-sillimanite-cordierite mineral assemblages in migmatitic sedimentary gneisses and partial melt development (750 ± 50 °C and 5.5 ± 1 kbar)(Kraus and Menard, 1997; White, 2005).

3 Deposit geology

The discovery of the Lynn Lake Ni-Cu deposit in the 1940s led to the development of a significant base metal and gold mining center in the LLGB and exploration continues to this day. Three of the largest

gold deposits within the LLGB were sampled as part of the current study: (1) MacLellan; (2) Gordon (formerly Farley Lake); and (3) Burnt Timber. Each of these gold deposits is hosted within the Wasekwan Group rather than the younger, overlying Sickle Group. The geology of each gold deposit is discussed below.

3.1 MacLellan deposit

The MacLellan deposit was an underground gold and silver mine in the 1980s after its initial discovery in the 1940s. Approximately 0.1 Mt of Au at 5.46 g/t Au were extracted during its brief (1986–1989) mining history (Staples et al., 2017). Multiple, discontinuous high-grade ore zones occur within a broader NE-SW trending and steeply dipping package of faulted Wasekwan Group meta-volcanic and lesser meta-sedimentary rocks. Total proven and probable reserves within the most recent assessment include 18.08 Mt at 1.63 g/t Au and 4.43 g/t Ag (0.947 Moz Au and 2.578 Moz Ag)(Staples et al., 2017).

Multiple auriferous and barren mineralization styles and vein-types have been identified at the MacLellan deposit (Figs. 5–6)(Augsten et al., 1986; Beaumont-Smith, 2003; Beaumont-Smith and Böhm, 2004, 2002; Glendenning et al., 2014; Hastie et al., 2018; Ma et al., 2000; Ma and Beaumont-Smith, 2001; Park and Lentz, 2002; Samson and Gagnon, 1995; Samson et al., 1999). One of the earliest mineralization styles correspond to isoclinally folded, centimetre-scale quartz veins and more cryptic zones of silica flooding with transposed alteration halos comprising fine to ultrafine arsenopyrite (± pyrrhotite ± pyrite) and biotite (Fig. 5c).

Thicker, laminated quartz-chlorite veins with coarse arsenopyrite also occur within some high-grade Au ore zones (Fig. 5a, d). Both arsenopyrite-bearing vein types and their associated biotite and chlorite alteration halos are isoclinally folded and transposed parallel to the main S_2 fabric (Figs. 5a–d; 6a–b), resulting in gold ore zones with abundant intrafolial and rootless folds and extensive boudinage. Arsenopyrite is an important visual indicator of high-grade ore zones at the MacLellan deposit. However, coarse visible gold is rarely observed in this mineralization style, which may suggest that gold within these zones is structurally bound within arsenopyrite (Hastie et al., 2018). Multiple examples of each arsenopyrite

texture type were sampled for Re-Os geochronology and Pb isotope and trace element geochemistry as part of the current study (i.e., vein-hosted versus replacement-style arsenopyrite).

Base metal quartz-carbonate veins represent a third vein type at the MacLellan deposit. These veins often host abundant pyrite, pyrrhotite, sphalerite, galena, (Fig. 5f) and more rarely arsenopyrite and coarse visible gold. Because galena is argentiferous, base metal-rich veins comprise an important component of the Ag resource at the MacLellan deposit (Staples et al., 2017). All of these veins have a pre- to syn-D_2 timing that is similar to the gold-only veins described above, but some of the most sulphide-rich base-metal quartz veins are brecciated and/or have a net texture- to massive sulphide-like appearance. The texture and polymetallic signature of these veins, coupled with Zn-, Pb- and Ag-bearing mineralized zones that are locally decoupled from gold ore zones at the deposit scale, share some similarities with VMS-style mineralization (Fedikow and Gale, 1982). Gold ore zones also yield anomalous Ni-rich (e.g., pentlandite) concentrations and detailed mineralogical studies have documented a range of ultrafine Sb (tetrahedrite ± polybasite ± pyargite ± geocronite ± breithauptite ± ullmannite)- and/or Ag (Ag-rich electrum ± argentopentlandite)-bearing minerals that are somewhat unusual for other gold deposits in the LLGB and globally (Augsten et al., 1986).

The relative timing of folded and transposed veins with the S_2 fabric suggest a pre- to syn-D_2 timing for all three auriferous veins types and mineralization styles (Beaumont-Smith and Böhm, 2004, 2003, 2002; Hastie et al., 2018; Ma et al., 2000; Ma and Beaumont-Smith, 2001; Peck et al., 1998). However, most of the coarse visible gold grains observed in the present study occur in massive and decussate-textured amphibole, chlorite, carbonate, and pyrite alteration zones (Fig. 5b). Coarse visible gold within these amphibole + chlorite alteration zones typically occurs in the absence of sulphide and veining, which is unlike the other mineralization styles described above. Previous studies have interpreted these texturally and mineralogically distinct zones as post-D_2 due to the massive appearance of fine grained chlorite and the randomly oriented texture of the coarse-grained amphibole (Hastie et al., 2018; Samson et al., 1999). Chlorite and amphibole also appear to overprint biotite-rich halos in the areas where both alteration assemblages are present, which is consistent with a relatively late timing for overprinting amphibole +

chlorite alteration. New field observations, however, demonstrate that these zones are locally deformed and transposed by the S_2 fabric (Fig. 5b). As will be discussed below, the regional S_2 fabric is likely a composite structure that was multiply reactivated for tens of millions of years. Individual hydrothermal or alteration events, even if temporally distinct, may therefore be impossible to recognize using the S_2 fabric as a relative timing marker and in the absence of precise and spatially resolved (i.e., *in situ* analysis) geochronological constraints. Barren quartz, quartz + carbonate, quartz + carbonate + chlorite and quartz + amphibole + chlorite veins are also reworked by S_2, suggesting that auriferous fluids represent one component of a broader period of hydrothermal activity that likely overlapped in time with the main period of deformation (D_2).

Post-D_2 fabrics are also locally developed in drill core at the MacLellan deposit (Fig. 5e). Pyrite, pyrrhotite, and chalcopyrite are concentrated within the S_3 fabric where present, possibly pointing to overprinting hydrothermal alteration on pre- to syn-D_2 veins. These fabrics are relatively common in drill core intervals comprising biotite schist (Fig. 5e). Because pyrite-bearing S_3 fabrics were only recognized adjacent to pre- to syn-D_2 veins, it is possible that post-S_2 sulphide replacement reflects late remobilization rather than a younger hydrothermal alteration event. Minor remobilization of Au is also inferred from its late paragenesis at the micro-scale and the apparent importance of intersecting D_2 and post-D_2 structures as structural controls at the deposit-scale (Hastie et al., 2018). Post-D_2 quartz and quartz-calcite veinlets observed in core typically have sericite and calcite alteration halos that overprint biotite and/or chlorite-amphibole alteration styles, and, in the absence of pre- to syn-D_2 veins, are devoid of gold.

3.2 Gordon deposit

Prospectors discovered gold occurrences around the Gordon deposit in the 1940s, which ultimately led to a brief open-pit mining operation between 1996 and 1999 (Staples et al., 2017). Total proven and probable reserves from the most recent assessment suggest that the Gordon deposit contains approximately 8.72 Mt at 2.42 g/t Au (0.678 Moz Au)(Staples et al., 2017). The deposit is hosted by a steeply N- to NW-dipping BIF of the Wasekwan Group. The moderate to shallow S-dipping geometry of the ore zones (25–

45°) relative to the steeply dipping $S_0/S_1/S_2$-fabric suggests that auriferous fluids at Gordon may significantly post-date other pre- to syn-D_2 gold deposits within the LLGB (Beaumont-Smith, 2003; Beaumont-Smith et al., 2000; Peck et al., 1998). Shallow- to moderately-dipping quartz veins that cut north to northwest-trending open F_4 chevron folds are also consistent with a post-D_2 timing, although it is unclear whether these veins were mineralized (Beaumont-Smith et al., 2000). The hydrothermally altered and deformed (D_2) dioritic intrusion at the southern edge of the past-producing open pit yielded a U-Pb zircon crystallization age of 1854 Ma, which provides a maximum age estimate for gold mineralization (Lawley et al., 2018).

Two mineralization styles were recognized at the Gordon deposit: (1) pyrite + pyrrhotite replacement of magnetite-rich BIF (Fig. 5j); and (2) quartz + sulphide (pyrrhotite ± pyrite) + carbonate + amphibole veins (Fig. 5i). Vuggy pyrite veins with massive to semi-massive pyrrhotite and coarse visible gold intersect the main deposit fabric (S_2) at high angle (Fig. 5j). Pyrite and/or pyrrhotite alteration halos at the margins of these veins also locally define an S_3 fabric, which has been previously been interpreted to reflect a late structural timing for the Gordon deposit. However, multiple other lines of evidence support a pre- to syn-D_2 timing for gold mineralization: (1) moderately- to flat-dipping veins with coarse visible gold are locally folded and transposed by S_2 in drill core; (2) pre- to syn-D_2 veins (quartz + chlorite + amphibole) that are isoclinally folded or boudinaged are also a ubiquitous feature of the high-grade ore zones; (3) shallow-dipping auriferous quartz veins host the peak-metamorphic mineral assemblage (i.e., actinolite + grunerite + chlorite; Fig. 6c–f), which elsewhere in the LLGB has a broad syn-D_2 timing,; and (4) coarse visible gold occurs within some steeply dipping quartz-chlorite-amphibole veins that have a pre- to syn-D_2 relative timing (Fig. 5i).

Two possible scenarios are provided to explain these apparently contrasting field relationships: (1) gold was introduced pre- to syn-D_2 with minor remobilization into post-D_2 veins and fabrics. If correct, the shallow- to moderately-dipping geometry of the Gordon ore zones suggest that progressive D_2 deformation and subsequent events did not significantly impact the deposit geometry, which is unlike the extensive transposition and structural reworking at the other deposits within the LLGB; and/or (2) gold was initially

introduced pre- to syn-D_2 and then subsequently overprinted by a second generation of shallow-dipping veins and gold ore zones that post-date the main stage of D_2. Multiple pyrite samples from replacement and vein-hosted mineralization styles (pre- to syn-D_2 and post-D_2) were collected in an attempt to provide absolute timing constraints on the Au mineralization at the Gordon deposit.

3.3 Burnt Timber deposit

Drill core availability was limited at Burnt Timber relative to the MacLellan and Gordon deposits. Burnt Timber was also not included in the most recent mineral reserve estimate (Staples et al., 2017). However, the geology and mining history of Burnt Timber have been previously described (Anderson and Böhm, 2001; Beaumont-Smith, 2000; Jones et al., 2006, 2000; Peck et al., 1998). Gold was initially discovered in the 1980s before going into production between 1993 and 1996 as an open pit operation (Staples et al., 2017). The deposit is hosted by a W-trending and steeply dipping package of hydrothermally altered (e.g., biotite, ankerite, quartz, pyrite, chlorite, sericite) mafic meta-volcanic rocks and lesser interflow meta-sedimentary rocks of the Wasekwan Group.

High-grade gold ore zones are locally associated with pre- to syn-D_2, hydrothermally-altered (calcite + ankerite + sericite + pyrite + arsenopyrite) felsic feldspar porphyry dykes (Fig. 5h)(Jones et al., 2006, 2000). Multiple quartz veins types are present at Burnt Timber, including (1) narrow unmineralized quartz-pyrite veins, (2) auriferous quartz + carbonate + sulphide (pyrite ± chalcopyrite ± arsenopyrite ± galena) + biotite + chlorite veins, and (3) late-stage, unmineralized quartz + pyrite + chlorite veins (Jones et al., 2006). Mineralized quartz veins and hydrothermally altered host rocks within the high-grade Au ore zones are transposed, boundinaged, and isoclinally folded parallel to the main S_2 deposit fabric (Fig. 5g). Three pyrite samples were collected from pre- to syn-D_2 quartz + carbonate veins (n = 2) and their pyrite-rich alteration halo (n = 1).

4 Methods

4.1 U-Pb detrital zircon geochronology

U-Pb detrital zircon geochronology was completed at the Geological Survey of Canada, Ottawa, using the Sensitive High Resolution Ion Microprobe (SHRIMP). All six samples were crushed and milled in mild steel prior to mineral separation using a combination of Wilfley Table, density (Methylene Iodide) and magnetic techniques (Frantz™ isodynamic separator). Non-magnetic zircon grains were then hand-picked under ethanol and imaged using a Zeiss Evo 50 Scanning Electron Microscope (SEM) in back-scattered electron (BSE) and cathodoluminescence (CL) modes.

Analytical procedures are described in Stern (1997). Multiple crystals of primary (i.e., 6266; $^{207}Pb/^{206}Pb$ age = 559 Ma) and secondary (i.e., 1242; $^{207}Pb/^{206}Pb$ = 2679.8 ± 0.2 Ma)(Davis et al., 2019) zircon standards were mounted with unknowns and gold-coated prior to analysis. Isotopic ratios were measured using single electron multiplier in pulse counting mode. Spot size depended on the zircon morphology and texture, but ranged from 9 × 12 μm to 17 × 23 μm. Data were processed offline using SQUID (v. 2.5) software (Ludwig, 2009). No fractionation correction was applied to the Pb-isotope data. Common Pb correction utilized the Pb composition of the surface blank (Stern, 1997). The SHRIMP analytical data are reported in supplementary material Table 1. Detrital zircon weighted average ages were calculated using Isoplot v. 4.10 (Ludwig, 2009) and are reported with errors at the 2σ level of uncertainty.

4.2 Sulphide mineral separation

Arsenopyrite, pyrite, and pyrrhotite mineral separates were prepared at the Geological Survey of Canada using an approach that minimizes contact with metal. Samples were coarsely crushed in plastic with a plastic-wrapped hammer until approximately 90% of material passed through a 500 μm nylon sieve. Crushed material was then transferred to an agate mortar and milled in an ethanol slurry for 10 minutes. The median grain size of the sulphide powders following this approach was approximately ≤ 20 μm based on laser diffraction analysis with a Beckman Coulter LS 13 320 particle size analyzer. Sulphide powders were then purified using a combination of density (i.e., Methylene Iodide) and magnetic (i.e., Frantz™ isodynamic separator) mineral separation methods. Finally, non-magnetic sulphide powders were split into three aliquots for: (1) Re-Os geochronology; (2) Pb isotope analysis; and (3) trace elements analysis.

4.3 Re-Os arsenopyrite and pyrite geochronology

Re-Os sulphide geochronology was completed at the Durham Geochemistry Center, Department of Earth Sciences, Durham University (Lawley et al., 2013). Sulphide mineral separates were weighed and loaded in to Carius tubes (Shirey and Walker, 1995), with a known amount of Re-Os tracer solution (spike) that contains a known ^{185}Re and ^{190}Os abundance and isotopic composition. Spike samples were digested in a reverse aqua regia solution (11N HCl:15.5N HNO3) at 220°C for 24 h. Room-temperature solvent extraction and micro-distillation were used to isolate Os from the acid mixture; whereas Re was isolated using NaOH-acetone solvent extraction and anion chromatography. Purified Re and Os aliquots were then loaded on Ni and Pt filaments, respectively, prior to thermal ionization mass spectrometry (TIMS) using a Thermo Scientific TRITON mass spectrometer. Isotopic compositions for Re and Os were measured by static Faraday collection and in peak-hopping mode on a secondary electron multiplier, respectively. Analytical uncertainties are propagated and incorporate uncertainties related to Re and Os mass spectrometer measurements, isotopic composition, abundance of the blank, spike calibrations, reproducibility of standard Re and Os isotope values, and decay constant uncertainty (1.666×10^{-11} yr^{-1})(Smoliar et al., 1996). Standard solutions of Re (i.e., zone-refined Re ribbon) and Os (i.e., Durham Romil Osmium Standard, DROsS) were analyzed during each analytical session in order to monitor long-term mass spectrometry reproducibility. The Os standard measurements recorded in this study (e.g., $^{187}Os/^{188}Os = 0.1608 \pm 0.0001$ 2σ; n = 7) are identical to the long-term average $^{187}Os/^{188}Os = 0.16095$ (± 0.00097 2σ). The Re standard measurements recorded in this study (e.g., $^{185}Re/^{187}Re = 0.5988 \pm 0.0006$ 2σ; n = 7) are within uncertainty at 2σ to the long-term Re standard average $^{185}Re/^{187}Re = 0.59811$ (± 0.00296 2σ). Weighted averages were calculated using Isoplot v. 4.10 and are reported with errors at the 2σ level. All Re-Os analytical results are reported in supplementary material Table 2.

4.4 Pb isotope analyses

Pb isotope analyses were completed at the Isotope Geochemistry and Geochronology Research center (IGGRC; Department of Earth sciences, Carleton University) following Cousens (1996). Mineral separates were dissolved in a mixture of concentrated HF and HNO_3. The residue was then re-dissolved in a mixture of HNO_3 and HCl prior to further chemical separation. Isotope ratios were measured by TIMS (Thermo Scientific TRITON) and are corrected for fractionation using the NBS 981 standard values of Todt et al. (1996).

Replicate analyses of BCR-2 (n = 7) over the course of this study yielded Pb isotope ratios ($^{206}Pb/^{204}Pb$ = 18.744 ± 0.017; $^{207}Pb/^{204}Pb$ = 15.613 ± 0.020; $^{208}Pb/^{204}Pb$ = 38.693 ± 0.068; $^{208}Pb/^{206}Pb$ = 2.0642 ± 0.0020; $^{207}Pb/^{206}Pb$ = 0.8329 ± 0.0006) that are in good agreement with their preferred values from GeoReM ($^{206}Pb/^{204}Pb$ = 18.754 ± 0.009; $^{207}Pb/^{204}Pb$ = 15.622 ± 0.005; $^{208}Pb/^{204}Pb$ = 38.726 ± 0.022; $^{208}Pb/^{206}Pb$ = 2.064 ± 0.001)(Jochum et al., 2005). The total range measured for NBS 981 in a 2 year period bracketing the analyses are (2σ uncertainty): ± 0.017 for $^{206}Pb/^{204}Pb$; ± 0.021 for $^{207}Pb/^{204}Pb$; ± 0.038 for $^{208}Pb/^{204}Pb$; ± 0.0021 for $^{208}Pb/^{206}Pb$; ± 0.00038 for $^{207}Pb/^{206}Pb$. The total procedural blanks were less than 50 picograms. Reported analytical uncertainties include corrections for mass bias, which are based on replicate analysis of NBS981. All analytical results are reported in supplementary material Table 3.

4.5 LA-ICP-MS trace element analyses

Sulphide mineral separates were mixed with a micro-crystalline cellulose binder (Sigma-Aldrich) and pressed into pellets (Specac 5 mm die; 2 tonnes for 5 minutes) prior to direct analysis by laser ablation inductively coupled plasma mass spectrometry (LA-ICPMS; Agilent 7700x ICP-MS coupled to a Photon Machines Analyte G2 193-nm excimer laser ablation system) at the Geological Survey of Canada. Pressed sulphide powders were ablated using a 40 µm laser spot and a fluence of 4.5 J/cm^2 at 10 Hz. The ablation aerosol was transported to the ICP-MS using 1 l/min He (MFC-1: 0.6 l/min; MFC-2: 0.4 l/min) and was mixed with approximately 1 l/min Ar. Analyses consisted of 40 s of background measurement prior to 60 s of ablation, and ~50 s of washout between samples. The instrument was tuned on NIST-612 to achieve > 9,000 cps/ppm ^{175}Lu (50 µm spot, ~7 J/cm^2 at 10 Hz), while minimizing the production of oxides (< 0.25%

for ThO+/Th+) and maintaining a U/Th signal intensity ratio of ~ 1.0. Details on the instrument setup are provided in supplementary material Table 4.

Concentrations were calculated from the time-resolved LA-ICPMS spectra using standard-sample-standard bracketing and the Glitter software package (Griffin et al., 2008). The United States Geological Survey (USGS) doped synthetic basalt glass standard GSE-1G was used as the primary calibration standard; whereas Fe was used as the internal standard based on its stoichiometric concentration for each of the targeted sulphide mineral separates. Pressed sulphide powder standards MASS-1 (USGS) was used as a qualitative control standard to monitor instrument performance and to demonstrate that using basaltic glass GSE-1G as the primary standard is appropriate for sulphide analyses. A second quality control standard, i.e., sulphide Cu standard OREAS-111, was milled and pressed into pellets using the same method as unknowns. Reference concentrations for primary and secondary standards were taken from the online geological and environmental reference materials database (GeoReM)(Jochum et al., 2005), except for OREAS-111 which was based on its certificate values for bulk powder analysis. Calibration of Te was based on an internal working value (GSE-1G = 279 ppm) calculated from repeated measurement of NIST610. Reported results represent the average of three replicate analyses for each sample. We note that the In concentrations reported in supplementary material Table 3 have not been corrected for the isobaric interference on ^{115}In from ^{115}Sn.

Replicate analyses of the quality control standard MASS-1 suggest that measurement repeatability is generally ≤ 10% (RSD) for most trace elements above the analytical detection limit. Exceptions include Se (11%) and Pd (12%). Measurement repeatability for OREAS-111 is considerably worse, although RSD is generally ≤ 20% for most trace elements above the analytical detection limit (exceptions include: Sn = 50%; Th = 61%). The poor measurement repeatability for OREAS-111 is somewhat expected given that the standard is certified for whole-rock analysis of Cu ores rather than microanalysis. It is possible that OREAS-111 contains micrometric mineral inclusions that were not effectively homogenized during milling and pellet making. Natural sulphide mineral separates likely contain similar inclusions and the relatively poor measurement repeatability of OREAS-111 may be more typical of unknowns.

Replicate analysis of MASS-1 further suggest that measured concentrations are typically within 20% of their accepted values for most elements (Co = 1%; Ni = 2%; Cu = 3%; Zn = 7%; As = 19%; Mo = 5%; Ag = 16%; In = 12%; Sn = 13%; Tl = 16%; Pb = 1%; Bi = 6%; Au = 15%). Exceptions include Cr (-86%), Se (37%), Cd (32%), Sb (-36%), and Te (34%). Concentrations for these elements should therefore be treated as semi-quantitative, particularly because several of these elements were also problematic for OREAS-111 (Cr = 44%; Te = 35%). Other problematic elements within OREAS-111 included Zn (36%) and Sn (31%). However, analytical accuracy for OREAS111 was generally good overall despite the relatively poor measurement repeatability discussed above (Co = 7%; Ni = 3%; Cu = 5%; As = 3%; Mo = 4%; Ag = 4%; Cd = 10%; In = 2%; Sb = 18%; W = 18%; Tl = 21%; Pb = 21%; Bi = 20%; Th = 3%; U = 10%). All sulphide geochemistry results and methods are presented in supplementary material Table 3 and supplementary material Table 4, respectively.

5 Results and interpretation

5.1 U-Pb detrital zircon geochronology results

Three meta-conglomerate samples were collected at the southern limit of the LLGB (17CL0714-1522; 18CL0809-1104; 18CL0812-1218); whereas one meta-conglomerate was sampled at the unconformable contact between the Sickle and Wasekwan Groups (17CL0715-1035)(Figs. 2–3). Other meta-conglomerate horizons are intercalated with cross-bedded meta-sandstone, suggesting a common depositional environment for both rocks types during Sickle Group sedimentation. Conglomerate clasts are well rounded and mostly comprise granite, quartzite, and quartz veins along with lesser conglomerate, sandstone, mudstone, and volcanic rocks. Many of these clasts were folded, hydrothermally altered, and possibly metamorphosed prior to sedimentation. With the possible exception of rare fuchsite-bearing volcanic and hematite-altered sedimentary rocks, most of the clasts within the conglomerate are fairly typical of the greenstone belts within the Reindeer zone. Sampling was focused on the sandy matrix of each conglomerate sample and excluded large clasts wherever possible. Meta-Psammite (17CL0718-0915) and -conglomerate (18CL0825-1525) samples from the northern LLGB were collected to test the timing of

rocks previously mapped as the Zed Lake greywacke and Ralph Lake conglomerate, respectively (Milligan, 1960). The timing relationship between these rock packages with the Sickle Group and the greenstone belts was not previously known

The results from six U-Pb detrital zircon samples are presented as part of the current study (Figs., 7–8). Zircon morphologies from mineral separates recovered from each sample were diverse and ranged from rounded, equant grains of obvious detrital origin to long, euhedral, and undamaged zircon crystals that were likely sourced from nearby rocks of igneous origin (Fig. 7). Oscillatory zoning was recognized in the majority of zircon crystals, although some obvious primary zoning was overprinted by metamict zircon domains (Fig. 7). Altered zircon domains were concentrated along fractures, grain boundaries, and/or replacing specific bands of the oscillatory zoning. In some of the most extreme cases, metamict zircon domains resulted in skeletal zircon structures. The most damaged zircon crystals were recovered from the meat-psammite sample 17CL0718-0915. A small subset of zircon grains also contain a bright (i.e., bright in back-scatter electron imaging) µm-thin rim that was too small to target with the spot sizes used in this study. A representative suite of zircon grains morphologies and textures from each sample were targeted for analysis (Fig. 7). After obtaining an initial age profile, the youngest zircon of each sample was then targeted for repeat analyses to constrain a maximum depositional age for the Sickle Group (Fig. 8). The Th/U ratio of the detrital zircons (Th/U mean = 0.43; standard deviation = 0.22; range = 0.01–1.65) tends to be higher than previously published results for metamorphic zircons (Th/U < 0.07)(Rubatto, 2002), which, coupled with their morphology and zoning patterns, suggests that most of the analyzed grains presented herein are igneous in origin.

Sickle Group conglomerate sample 18CL0809-1104 (analysis ID = 12404) yielded the youngest detrital zircon population. This sample was collected at the southernmost margin of the LLGB (Fig. 2). Six replicate analyses of the youngest concordant zircon grain yield a weighted average $^{207}Pb/^{206}Pb$ age of 1836 ± 15 Ma (MSWD = 1.3; n = 6; 12404-071; Fig. 7). This age is essentially identical to the youngest Sickle Group zircon, which is based on an unpublished and discordant (+8%) U-Pb TIMS single zircon $^{207}Pb/^{206}Pb$ age at 1830 ± 3 Ma (C. Böhm pers. comm.). One other young detrital zircon grain from sample 18CL0809-

1104 was not reproducible over three analyses, which resulted in an imprecise age with an unacceptably large MSWD (weighted average $^{207}Pb/^{206}Pb$ age at 1836 ± 150 Ma; MSWD = 150; n = 3). The next two youngest reproducible zircon grains recovered from this sample yield slightly older weighted average $^{207}Pb/^{206}Pb$ ages at 1854 ± 14 Ma (MSWD = 0.9; n = 7; 12404-007) and 1851 ± 13 Ma (MSWD = 0.3; n = 3; 12404-058). The vast majority of the remaining zircon grains yield a prominent $^{207}Pb/^{206}Pb$ age mode at ca. 1.86 Ga, which likely reflects a mixture of locally sourced detritus (1.90–1.87 Ga Wasekwan Group and Pool Lake igneous suite and the ca. 1.86–1.85 Ga Burge Lake igneous suite). Replicate analyses of one zircon grain yield a significantly older weighted average $^{207}Pb/^{206}Pb$ age at 2525 ± 5 Ma (n = 2; 12404-029; Fig. 7).

Cobble conglomerate sample 17CL0715-1035 (analysis ID = 12171) was collected at the unconformable contact between the Pool Lake igneous suite and the overlying Sickle Group at Hughes Lake (Figs. 2–3). This sample yielded multiple zircon grains with concordant $^{207}Pb/^{206}Pb$ ages ≤ 1.85 Ga, including weighted average $^{207}Pb/^{206}Pb$ ages at 1842 ± 13 (MSWD = 1.2; n = 9; 12171-065), 1843 ± 28 (MSWD = 1.8; n = 4; 12171-027), 1842 ± 13 (MSWD = 1.2; n = 9; 12171-065), and 1847 ± 8 (MSWD = 0.9; n = 5; 12171-141). Most of the remaining detrital zircons yield ages ranging from (1.90–1.86 Ga); whereas a smaller subset of analyses yield concordant $^{207}Pb/^{206}Pb$ ages at ca. 2.1, 2.4, 2.5, and 2.7 Ga. The dominant age mode and lesser subset of ca. 2.5 Ga zircon grains are similar to the age profile of the detrital zircon sample described above (Fig. 8).

The youngest two zircon grains within the Sickle Group quartz pebble conglomerate sample 17CL0714-1522 (analysis ID = 12170) yield weighted average ages of 1845 ± 13 Ma (n = 2; 12170-022) and 1852 ± 7 Ma (MSWD = 0.8; n = 4; 12170-066). This sample also yielded a prominent $^{207}Pb/^{206}Pb$ age mode at 1.86 Ga, with lesser modes at ca. 2.4 and 2.5 Ga. The detrital zircon age profile of this sample is in good agreement with the cobble conglomerate samples described above, which were collected lower in the stratigraphy of the Sickle Group (Fig. 8). One zircon yielded a significantly older concordant $^{207}Pb/^{206}Pb$ age at 3357 ± 8 Ma (12170-018).

Sickle Group cobble conglomerate sample 18CL0812-1218 (analysis ID = 12405) contained two zircon grains with concordant weighted average $^{207}Pb/^{206}Pb$ ages of 1842 ± 9 Ma (MSWD = 0.6; n = 6; 12405-010; Fig. 7) and 1849 ± 11 Ma (MSWD = 0.3; n = 6; 12405-041; Fig. 7). Both of these youngest detrital zircon ages overlap within analytical uncertainty at 2σ with the ≤ 1.85 Ga recovered from the other meta-conglomerate samples. The remaining detrital zircons yield a prominent $^{207}Pb/^{206}Pb$ ages age mode at 1.86 Ga and a few scattered $^{207}Pb/^{206}Pb$ ages at ca. 2.4, 2.5, and 2.7 Ga (Fig. 8).

Zircons recovered from the northern Sickle Group psammite sample 17CL0718-0915 (analysis ID = 12172), which is part of the previously defined Zed Lake greywacke (Milligan, 1960), were smaller and more metamict than the other samples, which required a smaller spot to target the relatively small surface area of pristine domains. Because of the smaller spot size, individual U-Pb ages are associated with a relatively large analytical uncertainty and replicate analyses of the youngest zircon grain were not attempted for this sample. However, the age profile of sample 17CL0718-0915 is similar to the more precise detrital zircon ages recovered from the Sickle Group, including a prominent mode at ca. 1.86 Ga and lesser Paleoproterozoic to Archean zircon grains (Fig. 8).

Replicate of the youngest zircons recovered from the Ralph Lake conglomerate sample 18CL0825-1525 (analysis ID = 12407) yield a weighted average $^{207}Pb/^{206}Pb$ age at 1849 ± 30 Ma (MSWD = 2.7; n = 8; 12407-016). The relatively large MSWD for this youngest detrital zircon is due to one anomalously young analysis. If excluded, the remaining analysis yield a slightly older, but more precise weighted average $^{207}Pb/^{206}Pb$ age at 1857 ± 16 Ma (MSWD = 1.1; n = 7; Fig. 7). This age is essentially identical to the next youngest detrital zircons, including weighted average $^{207}Pb/^{206}Pb$ ages at 1858 ± 8 Ma (MSWD = 2.1; n = 8; 12407-057) and 1860 ± 16 Ma (MSWD = 1.7; n = 7; 12407-026). The maximum depositional age and prominent $^{207}Pb/^{206}Pb$ age mode at ca. 1.86 Ga is thus very similar to Sickle Group samples (Fig. 8). The few older detrital zircon ages for the Ralph Lake conglomerate at ca. 2.4, 2.5, 2.7, and 3.0 Ga are also similar to the other dated samples (Fig. 8). Together, the available age results suggest that the Ralph Lake and Sickle Group conglomerates were broadly coeval and contain detritus of similar age provenance.

5.2 Re-Os geochronology results

Multiple arsenopyrite, pyrite and/or pyrrhotite mineral separates were prepared (n = 38) from three deposits (i.e., MacLellan, Gordon, and Burnt Timber). Of these, only 19 samples yielded sufficient Re to attempt Re-Os dating (total analyses = 23; Fig. 9). Arsenopyrite and pyrite results scatter about a ca. 1.8 Ga errorchron (1794 ± 18 Ma; 2σ; MSWD = 159; n = 15; York model 3; initial $^{187}Os/^{188}Os$ = 1.0 ± 0.9). Reproducible replicate analyses suggest that this excess data-point scatter reflects disparate sulphide generations rather than an analytical artifact (supplementary material Table 2).

Sulphide samples that yield high $^{187}Re/^{188}Os$ ratios (> 5000) and/or calculated $^{187}Os^{r}$ concentrations (> 98%) are highly radiogenic, suggesting that nearly all of the measured ^{187}Os is due to the radiogenic decay of ^{187}Re with minimal contribution of common ^{187}Os (Lawley et al., 2015, 2013; Stein et al., 2000). For these highly radiogenic arsenopyrite and/or pyrite samples, model ages can be calculated in a manner that is similar to molybdenite model ages (Fig. 9). Two replicate analyses of the two arsenopyrite samples with the highest $^{187}Re/^{188}Os$ (6132–16564; n = 4) yield weighted average Re-Os model ages at 1824 ± 12 (n = 2) Ma and 1782 ± 16 Ma (n = 2). Both of these ages are relatively insensitive to the choice of initial Os composition. The older ca. 1.82 Ga arsenopyrite sample was taken from a pre- to syn-D_2 quartz-sulphide vein at the MacLellan deposit; whereas the younger ca. 1.78 Ga arsenopyrite sample was collected from sulphide- and biotite-altered host rocks adjacent to a pre- to syn-D_2 quartz-sulphide vein at the same deposit (Fig. 9). Both of these ages were obtained from coarse arsenopyrite porphyroblasts and within analytical uncertainty of previously published U-Pb xenotime and monazite ages from the same deposit (Lawley et al., 2019). Replicate analyses of one highly radiogenic pyrite sample ($^{187}Re/^{188}Os$ = 694–1005; $^{187}Os^{r}$ = 98%) represent the best available timing estimate for sulphide replacement from the Gordon deposit at 1838 ± 28 Ma (n = 2). A regression through the three reproducible arsenopyrite and pyrite samples from the MacLellan and Gordon deposits yield a York Model 1 Re-Os isochron age of 1823 ± 4 Ma (MSWD = 1.5; n = 6; initial $^{187}Os/^{188}Os$ = 0.60 ± 0.02).

The remaining arsenopyrite and pyrite analyses are moderately to highly radiogenic ($^{187}Os^{r}$ = 57–99%), but scatter to lower $^{187}Re/^{188}Os$ ratios (57–2418) and yield a broad range of Re-Os model ages (1980–

764 Ma; Fig. 9). For samples that contain a small but variable proportion of common Os, Re-Os model ages should be regarded as minimum ages. A subset of the older pyrite analyses from the MacLellan deposit (≥ 1.83 Ga) yield a York Model 1 Re-Os isochron age of 1865 ± 21 Ma (MSWD = 0.04; n = 4; initial $^{187}Os/^{188}Os = 0.48 \pm 0.06$). Two of these three samples share a similar paragenesis (i.e., pyrite-rich biotite schist), which may suggest that the oldest Re-Os model ages reflect early-sulphide deposition that pre-dates regional metamorphism. However, pyrite mineral separate with older apparent ages are associated with large analytical uncertainties and one sample within this potential group was collected adjacent to veins that yield Re-Os model pyrite ages older than the host rock, which likely reflects isotopic disturbance. A subset of anomalously young samples, including the two samples from Burnt Timber, yield model ages that cluster around ca. 1.3 and 0.8 Ga (Fig. 9). These ages are considerably younger than any of the previously published ages for the THO. Anomalously young Re-Os model ages may reflect disturbance and/or variable resetting to produce geologically meaningless dates. Alternatively, young pyrite ages reported herein may reflect young fluids that circulated during Meso- to Neoproterozoic re-heating and/or some other form of cratonic instability (McDannell et al., 2018). The young tectonothermal history of the THO was previously identified using K-feldspar thermochronology ($^{40}Ar/^{39}Ar$ multi-diffusion domain analysis)(McDannell et al., 2018), but, prior to this study, has not been reproduced by other isotopic dating methods. Because of some evidence for Re-Os disturbance in the sulphide samples that yield old apparent "ages" (i.e. pre-date ca. 1.83 Ga) and the uncertain geological significance of the youngest sample subset, the reproducible Re-Os model ages for the two highly radiogenic samples from the MacLellan deposit represent the preferred timing for sulphidation in the LLGB (ca. 1.82 and 1.78 Ga; Fig. 9).

5.3 Pb isotope and trace element results

Sulphide (i.e., arsenopyrite, pyrite and pyrrhotite) mineral separates prepared for Re-Os dating yield a range of $^{206}Pb/^{204}Pb$ (15.468–46.414), $^{207}Pb/^{204}Pb$ (15.164–18.830) and $^{208}Pb/^{204}Pb$ (35.029–44.581) ratios (n = 38). The available data scatter around Paleoproterozoic secondary errorchrons (not shown), which is consistent with the inferred timing of sulphidation (i.e., 1.82–1.78 Ga; discussed above) and points

to significant radiogenic in-growth of Pb after sulphide deposition. To correct for the growth of radiogenic Pb, measured Pb isotope ratios were back-projected along secondary 1.8 Ga isochrons to intersect the Stacey and Kramers (1975) primary isochron at 1.8 Ga. The intersection of primary and secondary isochrons represent the best available estimate for the Pb isotope composition for each sample at 1.8 Ga (Fig. 10). Uncertainty over the true age of the sulphide mineral separates has the potential to add scatter to the calculated initial Pb isotope compositions; however, the broadly co-linear distribution of all samples along Paleoproterozoic secondary Pb errorchron suggests that Meso- to Neoproterozoic sulphides, if present, did not significantly impact the U-Pb systematics. The calculated range of initial Pb isotope compositions (i.e., U/Pb) is more likely to reflect mixing between depleted mantle-like (i.e., low-μ) and crust-like (high-μ) end-members.

Age-corrected Pb isotope compositions ($\mu_{1.8\ Ga}$) range from 8.9–10.6, which extend from depleted to enriched U/Pb ratios relative to the terrestrial silicate curve (i.e., $\mu = 9.7$; Fig. 10)(Stacey and Kramers, 1975). Least radiogenic samples are similar to the composition of juvenile, mantle-derived magmas in the THO (Arndt and Todt, 1994), whereas the more radiogenic Pb isotope signatures are similar to global models for the isotope composition of the crust and galena from nearby volcanogenic massive sulphide deposits (Sangster, 1978).

Aliquots of each mineral separate were also milled and pressed into pellets prior to trace element analysis by LA-ICPMS. Integrating trace element data, Re-Os geochronology, and age-corrected Pb isotope data for the same sample suite provide new constraints on the timing and composition of the ore fluids. Arsenopyrite analyses from the MacLellan deposit yield the greatest concentrations for Au + Ag + Pb + Zn ± Cd ± In ± Sb (Fig. 10). Part of this compositional range is likely due to micro-inclusions of native Au, galena and sphalerite that remained in arsenopyrite after mineral separation and were mixed during pellet making.

Pyrite from the MacLellan and Burnt Timber deposits are somewhat less radiogenic and, with the exception of As + Ni + Co + Cu (± Pt ± Pd), are mostly trace-element poor (Fig. 10). Pyrite analyses from Gordon trend towards more radiogenic Pb isotope compositions and are also relatively Bi + Te enriched

(± Mo; Fig. 10). These elements likely occur as telluride and/or bismuthide minerals, which occur with Au at the micro-scale (Fig. 6c–f). The trend from least- to most radiogenic pyrite analyses from both deposits may point to variable mixing between depleted mantle-like and more radiogenic crust-like fluid components ($\mu_{1.8\ Ga} \geq 9.74$)(Stacey and Kramers, 1975). Radiogenic fluids appears to have introduced Re, possibly due to the precipitation of ultrafine molybdenite and/or other very fine grained Re-bearing phases that were not apparent during petrography (e.g., germanite and renierite)(Selby et al., 2009). It is possible that molybdenite inclusions, if present, may have contributed to the complex distribution of Re-Os model ages (Fig. 10). The origin of these radiogenic fluids is also unclear and could represent U-rich magmatic fluids and/or metamorphic fluids that interacted with sedimentary rocks prior to precipitating radiogenic pyrite and arsenopyrite. Hydrothermal fluids that interacted with sedimentary rocks, particularly organic-rich sediments that are likely present at Gordon as BIF and argillite, provide an alternative explanation for the Re-enrichment observed within the more radiogenic sulphide samples (Fig. 10) (Kendall et al., 2009; Morelli et al., 2005; Selby et al., 2009).

6 Discussion

6.1 Synorogenic sedimentary basins

Detrital zircon ages are an important record of orogenesis that can track the uplift, erosion, and paleogeography of evolving mountains systems (Cawood et al., 2012). In the LLGB, meta-arkose, -psammite, and -conglomerate comprising the Sickle Group unconformably overlie 1.90–1.87 Ga mafic meta-volcanic rocks of the Wasekwan Group and the 1.89–1.87 Ga Pool Lake igneous suite (Fig. 3) (Baldwin et al., 1987; Beaumont-Smith et al., 2006; Beaumont-Smith and Böhm, 2004, 2002; Milligan, 1960; Norman, 1934). This unconformable depositional relationship, coupled with rare cross-bedded meta-psammite, coarse meta-arkose, local hematite-colouring and boulder- to pebble-sized clasts of previously deformed quartzite and gneiss, suggest that the Sickle Group was deposited in a fluvial and/or alluvial environment (Fig. 4)(Gilbert et al., 1980; Zwanzig et al., 1999). Felsic to mafic dykes and plutons intrude the Sickle Group and provide minimum depositional ages, however, the precise timing of sedimentation

has proven difficult to constrain in practise because many of the contact relationships between the Sickle Group and adjoining plutons are tectonized (Ansdell and Norman, 1995; Beaumont-Smith et al., 2006; Beaumont-Smith and Böhm, 2004, 2002; Connors et al., 1999; Machado et al., 1999; Maxeiner et al., 2005; Maxeiner and Morelli, 2014). Because of the uncertainty over these faulted contacts and despite being based on relatively high-precision TIMS U-Pb zircon ages, previously published minimum depositional ages for the Sickle Group have ranged from 1.85–1.83 Ga (Beaumont-Smith et al., 2006; Beaumont-Smith and Böhm, 2004, 2002). The few available, and mostly unpublished, detrital zircon ages for the Sickle Group did not define a maximum depositional age because these studies did not conduct replicate analyses of the youngest detrital zircon in each sample (Beaumont-Smith et al., 2006).

Six replicate analyses of the youngest detrital zircon reported herein provide the first reproducible maximum depositional age for the Sickle Group at 1836 ± 15 Ma (Figs. 7–8). This age mostly post-dates the 1.86–1.85 Ga Burge Lake intrusive suite, which coupled with the 1.86 Ga detrital age mode(Fig 8), suggests that these intrusions can be considered to be part of the pre-Sickle Group suite of intrusions (Beaumont-Smith et al., 2006). Sedimentation of the Sickle Group also post-dates the "successor-arc" plutons that are common throughout the Reindeer Zone (Syme, 1988). New maximal depositional ages that post-date the ca. 1.85 Ga Burge Lake suite intrusions may further suggest that the Sickle Group was deposited on the amalgamated Wasekwan-Pool Lake basement after the LLGB was already stitched to the Hearne cratonic margin (Fig. 11–12). If correct, this places the depositional setting of the Sickle Group on the southern Hearne cratonic margin prior to continent-continent collision with the Superior and/or Sask cratons (Figs. 1, 12). However, other authors suggest that the LLGB was still situated in an oceanic setting during emplacement of the Wathaman Batholith (Maxeiner et al., 2005) and that the Burge Lake igneous suite is related to on-going intraoceanic arc magmatism.

The new detrital zircon-based maximum depositional age overlaps within analytical uncertainty at 2σ with the ages of the youngest syn- and post-metamorphic dykes and plutons in the LLGB (ca. 1.83–1.78 Ga)(Beaumont-Smith and Böhm, 2004, 2002; Turek et al., 2000). Some of these intrusions, including the Fox Mine tonalite dated at 1831 ± 4 Ma (Turek et al., 2000) are interpreted to intrude the Sickle Group in

places (Beaumont-Smith and Böhm, 2004, 2002). If this intrusive contact relationship is correct, the Fox Mine tonalite provides a minimum depositional age to constrain the timing of Sickle Group sedimentation between 1836 ± 15 and 1831 ± 3 Ma (Figs., 2–3, 11–12). The Wasekwan and Sickle groups were metamorphosed to amphibolite facies by ca. 1814 Ma.

The slightly older maximum depositional age (1857 ± 16 Ma) for what was previously mapped as the Ralph Lake conglomerate overlaps with the ca. 1.85 Ga Burge Lake igneous suite. New detrital zircon ages for this sample are thus broadly consistent with the previously interpreted intrusive contact relationship between these meta-sedimentary rocks and the Burge Lake pluton (1857 ± 16 Ma)(Beaumont-Smith et al., 2006). If the interpretation of that intrusive contact is correct, the Ralph Lake conglomerate would be temporally distinct from the Sickle Group (1836 ± 15 to 1831 ± 4 Ma), suggesting at least two disparate meta-sedimentary packages (i.e., ≤ 1.86 and ≤ 1.84 Ga) and/or continuous sedimentation (i.e., 1.86–1.83 Ga) overlying the 1.90–1.87 Ga Wasekwan-Pool lake suite. Continuous deposition of the Sickle Group during this time period would be similar to the timing of the Kisseynew Basin, although more precise maximum depositional age constraints are required to test this hypothesis further. However, multiple ca. 1.85 Ga detrital zircons within all six dated samples instead suggest that 1.86–1.85 Ga plutons were eroding at the time of conglomerate and psammite sedimentation. If the Burge Lake pluton is in fact in faulted contact with the adjoining metasedimentary rocks, then rocks previously mapped as the Ralph Lake conglomerate and Zed Lake greywacke are more likely correlative with the Sickle Group (Fig. 2).

The similar detrital zircon age peaks within all six sample samples tend to support a common provenance, and thus similar depositional setting for all six detrital zircon samples and that is the preferred interpretation presented herein (Fig. 8). The prominent $^{207}Pb/^{206}Pb$ detrital zircon age modes for each sample (ca. 1.86 Ga) suggests that most of the detritus was sourced locally from the underlying Wasekwan Group, and the Pool Lake and Burge Lake ntrusion suites. Older ca. 2.12, 2.39, 2.51, 2.73, 3.02, and 3.35 Ga zircons likely require significant sedimentary transport because the potential Paleoproterozoic and Archean sources of this detritus are currently not exposed in the LLGB (Fig. 1–2). Some of these Meso- to Neoarchean zircons were presumably sourced from at least one of the adjoining cratons to the THO (i.e., Hearne and/or

Sask), or, somewhat less likely, from rare inherited zircons hosted within the eroding Paleoproterozoic igneous intrusions (Fig. 1). The minor mode of detrital zircons at ca. 2.51 Ga (Fig. 8) are particularly intriguing as these ages are typical of the Kaminak igneous event and coeval rocks within the Sask craton, which today is mostly buried over a hundred kilometers south of the LLGB (Ashton et al., 1999).

Immediately west of the LLGB, polymictic conglomerate and coarse, feldspathic and cross-bedded clastic sedimentary successions bordering the La Ronge belt were formerly mapped as the McLennan Group (Lewry, 1983; Maxeiner, 1999; Maxeiner and Demmans, 2000). Detrital zircon age peaks for the McLennan Group reflect locally sourced detritus from the unconformably underlying volcano-plutonic arc basement (e.g., prominent mode at 1.85 Ga) with young detrital zircon ages (i.e., 1835 Ma)(Maxeiner and Demmans, 2000) that are virtually identical to the maximum depositional age of the Sickle Group reported herein. More recently, coarse clastic sedimentary rocks in the southwestern La Ronge belt in Saskatchewan have been re-interpreted as the Mullock Lake lithotectonic assemblage (Maxeiner and Kamber, 2011; Maxeiner and Morelli, 2014). Detrital zircon age results from this newly defined sedimentary-igneous rock assemblage yield modes at ca. 1.89 and 1.85 Ga, similar to the Sickle Group (Maxeiner and Kamber, 2011).

South and east of the LLGB, meta-sedimentary rocks of similar age and provenance are known as the Missi and Grass River Groups, respectively (Ansdell et al., 1992; Bailes, 1980; Zwanzig, 1999). These coarse clastic meta-sedimentary rocks, along with amphibolite facies meta-sedimentary rocks of suspected marine origin within the intervening Kisseynew basin (e.g., alternating meta-greywacke and -mudstone deposits of the Burntwood Group), have been the subject of many previous studies (Ansdell et al., 1999, 1995, 1992; Ansdell and Norman, 1995; Connors et al., 1999; Machado et al., 1999; Zwanzig and Bailes, 2010; Zwanzig, 1999; Zwanzig et al., 2008). Around Flin Flon, Missi Group meta-psammite grades laterally into meta-greywacke of the Burntwood Group, suggesting that both meta-sedimentary packages were coeval (Zwanzig and Bailes, 2010; Zwanzig, 1999). The coeval timing of marine and clastic sedimentation is further supported by the youngest detrital zircon $^{207}Pb/^{206}Pb$ ages from the Missi (1837 ± 4 Ma) and Burntwood (1842 ± 2 Ma) groups, which overlap within analytical uncertainty at 2σ (Ansdell and Norman, 1995; Machado et al., 1999). Despite similar detrital zircon-based maximum depositional age estimates for

these meta-sedimentary rock packages, marine sedimentation within the Kisseynew basin may be as old as ca. 1855 Ma (David et al., 1996) and likely pre-dates, at least locally, alluvial-fluvial sedimentation unconformably overlying the LLGB (Ansdell et al., 1995; David et al., 1996; Machado et al., 1999; Zwanzig and Bailes, 2010).

Based on new and previously published results, a thin ribbon (10s of km) of broadly coeval, coarse clastic sedimentary clastic rocks of the Sickle Group and neighbouring correlative successions can be traced along strike across the Manitoba-Saskatchewan border and for 100s of km along the southern Hearne cratonic margin (Fig. 1). Interstratification of these alluvial-fluvial deposits with deep-water marine sedimentary facies were originally interpreted as rapid infilling of the Kisseynew basin at an active subduction margin (Ansdell et al., 1992; Connors et al., 1999; Zwanzig, 1999). If that interpretation is correct, the Sickle-Missi-Grass River-McLennan Groups and Mullock Lake assemblage would represent what were previously defined as molasse deposits in a foreland basin depositional setting (Ansdell et al., 1992). However, arc-like plutons that intrude the Burntwood Group may instead suggest that the Kisseynew basin formed in a back-arc (Ansdell et al., 1995). Coarse clastic sedimentary successions (e.g., Sickle-Missi-Grass River-McLennan Groups and Mullock Lake assemblage) that are coeval with the Burntwood Group and border the Kisseynew basin in that scenario would have been deposited on top of a previously deformed, but actively rifting oceanic setting (Ansdell et al., 1995). The geochemistry of plutons and dykes cross cutting the Sickle and Burntwood groups provide some of the few available constraints on the depositional setting of these synorogenic basins.

6.2 Syn- to post-Sickle Group intrusive suite

Magmatic rocks intrude both the Kisseynew basin and the coarse clastic sedimentary packages (Sickle-Missi-Grass River-McLennan Groups/Mullock Lake assemblage) unconformably overlying the older 1.90–1.85 Ga volcano-plutonic assemblages along the Hearne-Superior-Sask cratonic margins (Fig. 1). The composition and timing of these syn- to post-Burntwood and -Sickle Group intrusive suites provide critical constraints on the final assembly of the THO and have been the subject of extensive study (Bickford

et al., 2005; Hollings and Ansdell, 2002; Whalen et al., 1999; Zwanzig and Bailes, 2010). The oldest of these intrusive suites (1.84–1.83 Ga) yield a mixed, arc-like geochemical affinity (Fig. 12)(Hollings and Ansdell, 2002; Whalen et al., 1999; Zwanzig and Bailes, 2010). Because arc-like plutons (i.e., 1.84–1.83 Ga "boundary intrusions") (Ansdell et al., 1992; Machado et al., 1999) cut previously folded Missi Group rocks, fluvial-alluvial sedimentation continued after the initial stages of folding, faulting, and basin inversion (Fig. 12). Other syn- to post-Sickle Group intrusions (1.84–1.83 Ga) yield adakite- and/or sanukitoid-like to peraluminous compositions (Hollings and Ansdell, 2002; Whalen et al., 1999) that likely reflect different melt source regions during late-stage subduction and post-collisional magmatism. Some of the youngest detritus within the Sickle Group likely reflects erosion of these arc-like to post-collisional plutons.

Younger igneous intrusions (i.e., ≤ 1.83 Ga) yield a markedly different composition. These post-Sickle Group intrusive phases point to a significant shift in the evolution of the THO after basin inversion (Figs. 11–12)(Bickford et al., 2005; Hollings and Ansdell, 2002; Whalen et al., 1999; White, 2005; Zwanzig and Bailes, 2010). First, the unusual composition of the ultramafic to intermediate rocks of the 1830–1823 Ma Touchbourne intrusive suite points to a modified lithospheric mantle source region that is unlike the nominally older 1.84–1.83 Ga arc-like granitic intrusions within and at the margins of the Kisseynew basin (Ashton et al., 1999; Gordon et al., 1990; Machado et al., 1999). Second, syenitic and carbonatite intrusions are notably absent prior to ca. 1.83 Ga (Chakhmouradian et al., 2008; Martins et al., 2011). Alkaline rocks of this age intrude south and east of the LLGB (i.e., Eden Lake; zircon-bearing syenite yield ages 1831–1825 Ma; zircon-bearing carbonatite yield age at 1815 ± 8 Ma; Fig. 1)(Chakhmouradian et al., 2008; Elliott, 2009; Mumin and Corriveau, 2004), along the Superior cratonic margin (Chakhmouradian et al., 2009), and within the Kisseynew basin (Martins et al., 2012, 2011). These young alkaline intrusions were likely focused into the crust by translithospheric structures, as suggested by the position of the Eden Lake complex along strike of a major step in the upper mantle (Figs. 1–3; 12)(White et al., 2000). Widespread ultrapotassic and alkaline magmatism (i.e., Christopher Island Formation, ca. 1.83 Ga)(Cousens et al., 2002) within the Archean hinterland of the THO occurred at essentially the same time. Third, weakly peraluminous ca. 1.78–

1.77 Ga granite and pegmatite dykes document an increasing component of post-tectonic crustal melting after the burial of synorogenic basins (Figs. 11–12). Based on isotope studies, the crustal source regions of these pegmatite dykes must have included Archean basement or detritus, potentially after collision of the cratonic fragments bordering the THO (Bickford et al., 2005; White, 2005). These small, syn-to post-deformation tonalitic and pegmatitic dykes are the youngest intrusions in the LLGB and elsewhere (1.81–1.75 Ga)(Figs. 11–12).

6.3 Timing of gold mineralization

New Re-Os arsenopyrite and pyrite ages reported as part of the current study yield complex age profiles that require careful interpretation (Fig. 9). Older Re-Os model dates (1.98–1.83 Ga) are of uncertain significance due to the large analytical uncertainty for these moderately radiogenic mineral separates and since some of these apparent ages are older than the host rocks (Fig. 9). Given that the VMS mineralization (e.g., Fox mine) is hosted by the Wasekwan Group, it is possible, even likely, that some stages of hydrothermal alteration were coeval with mafic volcanism (1.91–1.85 Ga). In fact, the Zn- and Ag-rich ore zones at the MacLellan deposit were previously interpreted as sub-economic VMS alteration that was overprinted by orogenic gold-style mineralization (Fedikow and Gale, 1982). Unfortunately, the available Re-Os data does not allow this idea to be tested further. The oldest Re-Os ages have also not been reproduced by hydrothermal monazite and xenotime dating at the MacLellan deposit or elsewhere (Lawley et al., 2019).

The most robust age determinations correspond to Re-rich and highly radiogenic arsenopyrite and/or pyrite fractions with highly radiogenic Os isotopic compositions that are similar to data obtained from molybdenite (Stein et al., 2000). Unfortunately, only two arsenopyrite samples were sufficiently Re-rich and radiogenic to calculate Re-Os model ages. These samples yield reproducible Re-Os model ages at 1824 ± 12 Ma and 1782 ± 16 Ma, which represent the two preferred ages for the timing of sulphide deposition, and thus gold deposition at the MacLellan deposit (Figs. 9, 11–12). Critically, both Re-Os model ages also overlap with *in situ* U-Pb monazite and xenotime ages at the same deposit (Lawley et al., 2019).

Xenotime that occurs with native gold in a sulphide veinlet, which is isoclinally folded overgrown by garnet (Lawley et al., 2019), yield a weighted average $^{207}Pb/^{206}Pb$ age at 1827 ± 8 Ma (2σ; MSWD = 1.0; n = 15). The good agreement between monazite and arsenopyrite ages provides strong support for an early generation of auriferous fluids at the MacLellan deposit. This inferred 1824–1827 Ma hydrothermal and gold event immediately post-dates deposition of the Sickle Group, but pre-dates peak metamorphism in the LLGB at 1814–1801 Ma (Fig. 11)(Beaumont-Smith and Böhm, 2004, 2002).

The other highly radiogenic arsenopyrite sample yields a reproducible Re-Os model age at 1782 ± 16 Ma, which, coupled with coeval $^{207}Pb/^{206}Pb$ ages for monazite (1769 ± 2 Ma, MSWD = 0.9, n = 30) and xenotime (1807 ± 24 Ma, MSWD = 1.4, n = 13; 1796 ± 27 Ma, MSWD = 0.7, n = 4; 1791 ± 20 Ma, MSWD = 1.9, n = 20) at the same deposit, point to a punctuated hydrothermal and/or metamorphic history at the MacLellan deposit (Figs. 9, 11). The agreement between multiple geochronometers and minerals is important because it suggests that the younger generation of arsenopyrite at ca. 1.78 Ga is not related to an analytical artifact of the Re-Os method. The paragenesis of this sample is typical of the high grade ore zones and suggesting that multiple generations of arsenopyrite porphyroblasts and possibly gold are superimposed on the early auriferous veins. Replacement-style arsenopyrite- and gold-bearing mineralization is thus interpreted in some cases to overprint pre- to syn-D_2 hosted gold mineralization during a significantly younger hydrothermal event. The timing of late-stage arsenopyrite post-dates peak metamorphism at 1814–1801 Ma (Fig. 11), but is coeval with the pegmatitic to tonalitic dykes, the inferred timing of D_3, and a major regional thermal pulse at 1.78 Ga. Pegmatitic dykes with post-tectonic ages have previously been interpreted to reflect peak crustal thickening and/or some other sub-crustal heat source (Bickford et al., 1990). Late-stage arsenopyrite at the MacLellan deposit also immediately precedes the oldest biotite cooling ages at 1.77 Ga (O'Connor et al., 2019), suggesting that some auriferous veining occurred just prior to the LLGB cooling below peak amphibolite facies metamorphism.

Whether the other dated xenotime and monazite samples (1.81 Ga, 1.80 Ga, 1.79 Ga, and 1.77 Ga) reflect metamorphic mineral growth and/or additional stages of hydrothermal alteration is not clear in the absence of sulphide ages during this time interval. However, xenotime dated at 1.81–1.79 Ga that are either

overgrown by pyrrhotite and/or are concentrated at its margins demonstrates at least some sulphide mobility during peak metamorphism. The geological significance of moderately radiogenic sulphide mineral separates that scatter to significantly younger Re-Os model ages (ca. 1.3 and 0.8 Ga) is also uncertain.

The youngest xenotime at the MacLellan deposit ($^{207}Pb/^{206}Pb$ age at 1746 ± 12 Ma, MSWD = 0.7, n = 4) corresponds to the inferred timing of D_4. The few xenotime crystals of this age (ca. 1.75 Ga) post-date the oldest biotite cooling ages (ca. 1.77 Ga) and are hosted within a chloritized biotite schist, suggesting that some overprinting occurred during cooling and post-peak metamorphism (Fig. 11). However, these young xenotime grains and associated chlorite alteration are also interesting because they are aligned with the S_2 fabric at the MacLellan deposit and post-date both of the preferred arsenopyrite ages, suggesting that the D_2 structures controlling gold mineralization were repeatedly reactivated for 10s of Myr.

6.4 Sources of auriferous fluids

The Pb isotope signature of minerals with low to intermediate U/Pb ratios (e.g., arsenopyrite, pyrite and pyrrhotite) are a product of its initial composition and the *in situ* radiogenic decay of U. In the absence of precise age constraints, the Pb isotope composition of arsenopyrite and pyrite from ore samples have proven difficult to interpret. Herein we address that knowledge gap by integrating Re-Os, Pb isotope, and trace element chemistry for the same mineral separates (Fig. 10). Calculated Pb compositions at ca. 1.8 Ga are based on the intersection between secondary Pb isochrons for each sample with the primary 1.8 Ga isochron (Stacey and Kramers, 1975).

Two possible trends are apparent from the age-corrected Pb isotope and trace element composition of mineral separates: (1) MacLellan arsenopyrite mineral separates scatter to more radiogenic initial Pb isotope compositions and are relatively Au-, Ag-, Bi-, and Te-rich; whereas pyrite from the same deposit tend to yield more primitive initial Pb isotope compositions (Fig. 10); and (2) pyrite from the Gordon deposit tends to be more radiogenic than sulphide mineral separates from the other deposits and are also relatively Bi-, Te-, and Mo-rich (Fig. 10). At the microscale, bismuthides, tellurides, and native metals (Bi and Au) occur as ultrafine crystals intergrown with or fracture-fills in chlorite, amphibole, pyrite, and/or

arsenopyrite (Fig. 6). The microtextural setting of this ultrafine mineral assemblage is typical of metamorphosed gold ores and may be related to element remobilization during the metamorphic transition of pyrite to pyrrhotite (Lawley et al., 2017). Elements with low melting-points (e.g., Bi, Te) form native metals and alloys in such settings and it is possible that syn-metamorphic polymetallic melts or hydrothermal fluids may be responsible for scavenging and upgrading gold from early-stage pyrite and arsenopyrite. If correct, the radiogenic signature of mineral separates with a greater abundance of these remobilized native metals and alloys may be due to a crust-like fluid and/or polymetallic melt that is distinct from the more primitive hydrothermal fluids that precipitated early-stage arsenopyrite and pyrite. The isotopic differences between sulphide generations at the Gordon deposit is partially supported by the few pyrite samples from pre- to syn-D_2 veins that plots closer to veins of the same generation at the MacLellan and Burnt Timber deposits (Fig. 10). Unfortunately, some of the scatter around these inferred mixing lines is likely due to the heterogeneous distribution of alloys and native metals within the pressed powders. Future work should focus on producing finer and more homogenous mineral separate nanopowders, possibly through wet-milling methods and high-speed planetary ball mills (Lawley et al., 2020).

6.5 Sedimentary basin controls on orogenic gold deposits

Sedimentary basins that develop during the last stages of mountain building are a common feature of greenstone belts of all geological ages. In the Neoarchean Abitibi greenstone belt, the type locality, these synorogenic sedimentary basins are referred to as Timiskaming-type (Bleeker, 2015, 2012; Corfu et al., 1991; Hyde, 1980; Mueller and Donaldson, 1992). Some of the characteristic features of Timiskaming-type assemblages include: (1) deposition and/or preservation within long (i.e., discontinuous along strike for 100s of km), narrow, and fault-bounded basins that unconformably overlie significantly older and previously deformed meta-volcanic and -plutonic rocks; (2) alternating meta-sandstone and -mudstone intervals that likely represent deep-water, turbidite-like deposits of possible marine origin; (3) coarse clastic sedimentary rocks, including meta-conglomerate and -sandstone, that likely represent alluvial and/or fluvial deposits; (4) coeval calc-alkaline to alkaline volcanic and plutonic rocks derived, in part, from previously

metasomatized lithospheric mantle; and (5) a close spatial and temporal relationship with orogenic gold deposits along the two main deformation corridors (i.e., Larder-Cadillac and Destor-Porcupine faults).

Detailed structural analysis in the Timmins area suggests that the deep-water sedimentary facies of the Timiskaming assemblage was deposited during a synorogenic phase of extension (Bleeker, 2015, 2012). Deep penetrating faults that developed during this inferred extensional phase were interpreted by Bleeker (2012) as the ancestral structures that later focused auriferous fluids during the structural inversion of the Timiskaming-type basins (Fig. 12). Rapid burial by meta-conglomerate and -sandstone towards the stratigraphic tops of the Timiskaming-type basins was broadly coeval with the main stage of auriferous veining (De Souza et al., 2019). Continued shortening led to steepening of the basin-bounding structures and tectonic burial of the auriferous veins, which ultimately resulted in Timiskaming-type basins and gold deposits concentrated within the footwall of the two main gold-bearing deformation corridors (Fig. 12). According to this model, Timiskaming-type basins play an important genetic (i.e., fluid focusing along basin-bounding faults) and preservation control (i.e., rapid burial) on orogenic gold deposits (Bleeker, 2015, 2012). The empirical association between Timiskaming-type basins and orogenic gold deposits of multiple geological ages further suggest a common evolutionary stage during mountain building that is particularly favourable for this style of gold mineralization (Bleeker, 2015, 2012; Cameron, 1993; Groves et al., 1998; Kerrich and Wyman, 1990; Krapež and Barley, 2008; Maxeiner and Morelli, 2014).

Here we demonstrate that early-stage auriferous veins in the LLGB (1824 ± 12 and 1827 ± 8 Ma) immediately post-date the deposition of Sickle Group sediment (1836 ± 15 to 1831 ± 4 Ma). Turbidite-like rocks comprising the Burntwood Group (1855–1842 Ma) are locally interbedded with the Sickle Group, suggesting that these rocks are broadly coeval despite some older maximum depositional ages reported for the Kisseynew basin in some places (Zwanzig and Bailes, 2010). The close temporal relationship between marine turbidite-like deposits (i.e., Burntwood Group), alluvial-fluvial meta-sedimentary rocks (i.e., Sickle-Missi-Grass River and Mullock Lake assemblage), and early-stage gold deposition developed as part of the current study share a number of similarities with Timiskaming-type basins (Fig. 12). First, the ca. 24 Myr period (1855–1831 Ma; Burntwood and Sickle Groups) of basin opening and closing in this part of the

THO is very similar to the ca. 18 Myr series of events that define Timiskaming-type basins in their type locality (2687–2672 Ma synorogenic phase of extension; 2672–2669 Ma basin-inversion and filling; gold is locally ca. 2660 Ma)(Bleeker, 2015). Second, deposition of the Sickle Group was immediately followed by the first appearance of alkaline magmatism. Third, the thin ribbon of alluvial-fluvial sedimentary rocks (Sickle-Missi-McLellan groups and Mullock Lake assemblage) extends along strike for 100s of km and separates the highly prospective older volcanic rock packages from the poorly mineralized Kisseynew basin (Fig. 1). Finally, Sickle Group rocks were being deposited during basin inversion (ca. 1.83 Ga) and then buried and metamorphosed to amphibolite facies by 1814–1801 Ma. Rapid burial of early-stage auriferous veins by synorogenic Sickle Group sediments may represent an important preservation control for orogenic gold deposits in the LLGB.

However, unlike the Timiskaming-type basins, none of the known gold deposits or alkaline intrusions in the LLGB are actually hosted by the Sickle Group. Instead, the largest gold deposits in the LLGB are hosted by the meta-volcanic and -sedimentary rocks comprising the older and underlying Wasekwan Group along two main gold-bearing faults (Fig. 2). The local geological setting for mineralization in the LLGB thus contrasts with the close spatial distribution between Timiskaming-type basins and gold deposits in the structural footwall of the two main auriferous faults in the Abitibi greenstone belt. Deep-water meta-sedimentary rocks, which, in the Timiskaming-type basins represent one of the supporting pieces of evidence for the synorogenic extensional phase (Bleeker, 2015), are also mostly absent from the LLGB (Fig. 2). Immediately south of the LLGB in the Kisseynew basin, turbidite-like deposits comprising the Burntwood Group are locally coeval with the Sickle Group, but are almost entirely devoid of gold occurrences (Fig. 1).

The poor gold endowment of the Sickle and Burntwood Groups suggests that there is no special genetic relationship between orogenic gold and individual basin-bounding faults in the THO. Instead, deposition of the Sickle Group during inversion of a synorogenic extensional phase resulted in rapid infilling of the Kisseynew basin by coarse clastic sedimentary rocks of continental origin. The large number of gold occurrences that are associated with the thin ribbon (ca. 50 km wide) of meta-volcanic rocks and

synorogenic basin deposits at the margin of the Kisseynew basin are presumably related to repeated fluid focusing and favourable depositional traps within that large-scale geological setting (Fig. 1). The prospectivity of individual faults within this larger-scale geological setting may be unrelated to whether they were once basin-bounding structures.

The importance of large-scale architecture is further highlighted by the close temporal relationship between early-stage auriferous veins and the first appearance of alkaline magmatism. Although these syenite and carbonatite intrusions do not occur within the gold deposit stratigraphy (e.g., Eden Lake complex; Fig. 1), and are thus unlikely to have been the source of auriferous fluids, their timing points to an important shift in the magmatic history of the THO from arc- to lithospheric mantle- and/or crust-derived magmatism. Because early-stage auriferous veins pre-date most estimates for peak-metamorphism in the LLGB (1814–1801 Ma), upwelling asthenosphere and associated magmatism is the most likely driver for these hydrothermal fluids.

Crustal thickening during continental collision between the Hearne, Sask, and/ Superior cratons ultimately led to post-tectonic pegmatite dykes and other crustally-derived magmas during a post-peak metamorphic phase of magmatism. Late-stage arsenopyrite and gold (1782 ± 16 Ma) significantly post-dates peak metamorphism, but are coeval with this post-tectonic magmatic pulse and immediately preceded the onset of cooling. These pre- and post-peak metamorphic arsenopyrite ages are inconsistent with a local metamorphic-origin for auriferous fluids in the LLGB. However, the ultimate source(s) of gold and other ore components require further study. Whether monazite and xenotime ages sampled from the hydrothermally altered host rocks at the MacLellan deposit reflect additional hydrothermal, and possibly gold-bearing events, or a punctuated metamorphic mineral growth during a protracted period (1.81–1.75 Ga) of elevated metamorphic temperatures and pressures also remains unclear.

7 Conclusions

New U-Pb detrital zircon geochronology data constrain the depositional timing of the Sickle Group from 1836 ± 15 to 1831 ± 4 Ma. Early-stage auriferous veins (1824 ± 12 and 1827 ± 8 Ma) immediately

post-date closure and burial of these synorogenic basins. The close temporal relationships between deposition of the Sickle Group and auriferous veining is similar to the sequence of events established for Timiskaming-type sedimentary basins in the Abitibi greenstone belt, which points to a particular stage during mountain building that is highly prospective for orogenic gold deposits of all ages. However, the poor prospectivity of synorogenic basins themselves in the THO tends to suggest that individual basin-bounding faults are unlikely to have any special genetic or preservation control on orogenic gold deposits in the LLGB. Instead, the thin ribbon (ca 50 km wide and 100s of km long) of synorogenic sedimentary basins and highly prospective greenstone belts at the edge of the Kisseynew basin is more likely to reflect the favourable lithospheric architecture, repeated fluid focusing, and depositional traps at a reworked cratonic margin. Because early-stage auriferous veins are coeval with the switch from arc- to lithospheric mantle-derived magmatism and pre-date peak amphibolite facies metamorphism (1814–1801 Ma), upwelling asthenosphere and associated magmatism was the most likely driver for hydrothermal fluids. Late-stage arsenopyrite (1782 ± 16 Ma) post-dates peak metamorphism. The driver of late-stage hydrothermal fluids may have been heating during crustal thickening, as suggested by crustally-derived pegmatite dykes of this age, or some other unrecognized sub-crustal heat source. The contributions of early- versus late-stage hydrothermal events to the overall gold endowment of the LLGB is difficult to assess with the few available ages. Whether undated auriferous veins occurred during peak metamorphism also remains unclear. Nevertheless, the multi-stage hydrothermal history of the orogenic gold deposits within the LLGB demonstrates that reworked cratonic margins represent preferred pathways and depositional settings for auriferous fluids throughout the lifespan of an orogen.

Acknowledgements

This work was completed under the auspices of the Targeted Geoscience Initiative (TGI)-5 program and represents NRCan contribution number 20200142. The authors would like to thank the Manitoba Geological Survey and Alamos Gold for all of their logistical support and knowledge throughout the project. Discussions with Alamos Gold geologists were absolutely essential for the successful completion

of this research program. Adam Rhys O'Connor and Jordan Watts are thanked for their assistance with fieldwork. Wouter Bleeker, David Corrigan, Ralf Maxeiner, and one anonymous reviewer are thanked for their comments that improved an earlier version of this manuscript. We gratefully acknowledge the TOTAL Endowment Fund and the CUG Wuhan Dida Scholarship to DS, and analytical support from Antonia Hofmann, Geoff Nowell and Chris Ottley.

Figure Captions

Figure 1

Regional geological map of Saskatchewan and Manitoba [Saskatchewan geology polygons from the Saskatchewan Mining and Petroleum GeoAtlas; Manitoba geological polygons from Manitoba Mineral Resources (2013)]. Volcanogenic massive sulphide (VMS)(Galley et al., 2007), nickel-copper-platinum group-element (Eckstrand and Hulbert, 2007), gold deposits (Dubé and Gosselin, 2007), kimberlite (Kim.)(Faure, 2010) and carbonatites (Carb.)(Woolley and Kjarsgaard, 2008) are shown for reference. Gold occurrences are also shown for reference (data are commodity-filtered from the provincial mineral occurrence databases).

Figure 2

Local geology map of the Lynn Lake greenstone belt (Gilbert et al., 1980). Detrital zircon sample localities (this study), volcanogenic massive sulphide (VMS)(Galley et al., 2007), nickel-platinum group element (Eckstrand and Hulbert, 2007), and gold deposits (Dubé and Gosselin, 2007) are shown for reference.

Figure 3

Schematic stratigraphic column summarizing the main supracrustal groups and plutonic suites comprising the Lynn Lake greenstone belt. Ages are summarized from several sources (see text for further details). Abbreviations: BIF – banded iron formation; VMS – volcanogenic massive sulphides.

Figure 4

Photos of meta-conglomerate comprising the Sickle Group (a–d). Cobble to pebble sized clasts are generally well rounded and comprise previously deformed and metamorphosed volcanic and plutonic rocks. The Ralph Lake conglomerate (e–f) north of the MacLellan deposit contains a higher proportion of clasts of mafic to intermediate composition.

Figure 5

Core photo of veins and hydrothermal alteration from MacLellan (a–f), Burnt Timber (g–h), and Gordon (i–j) deposits. Gold (a–b and i–j) is often intergrown with amphibolite, chlorite, and/or pyrite. Arsenopyrite (c–d) is an important visual indicator of ore zones at the MacLellan deposit. Sulphidized (pyrite) biotite schist and base metal veins are locally gold-bearing. Auriferous shallow-dipping veins and their hydrothermal alteration halos at Gordon (j) are distinct from the other gold deposits in the LLGB. However, auriferous pre- to syn-D_2 veins also occur at Gordon (i). Gold ore zones at Burnt Timber are associated with hydrothermally altered meta-volcanic and –sedimentary rocks (g) and felsic dykes (h). Abbreviations: amphibole = Amph; arsenopyrite = Asp; biotite = Bt; calcite = Calc; chlorite = Chl; galena = Gn; pyrite = Py; pyrrhotite = Po; sphalerite = Sl; and quartz = Qtz.

Figure 6

Scanning electron microscope (SEM) backscattered electron (BSE) images of gold ore zones at MacLellan (a–b) and Gordon (c–f) deposits. Isoclinally folded and garnet-hosted sulphide veinlets (a) point to an early generation of hydrothermal mineral assemblages that are pre- to syn-metamorphic at the MacLellan deposit. Fine native gold are associated with early-stage hydrothermal alteration, but is often remobilized into low-strain micro-textural sites pre- to syn-S_2 (b). At Gordon, gold is intergrown with amphibole, chlorite and pyrite and often associated at the microscale with an unusual suite of Bi- and Te-bearing mineral phases. Some of these minerals remain unidentified and require further study. Concentrations are semi-quantitative

and based on energy dispersive spectrometry (EDS). Abbreviations: Amphibole = Amph; arsenopyrite = Asp; biotite = Bt; =bismuthinite = Bis; calcite = Calc; garnet = Gt; ilmenite = Ilm; magnetite = Mt; pyrite = Py; and quartz = Qtz.

Figure 7

Scanning electron microscope (SEM) backscattered electron (BSE) images of detrital zircons. Geochronology results are reported as weighted average $^{207}Pb/^{206}Pb$ ages for replicate analyses (i.e., multiple spots on same grain or multiple analyses on same spot) of each zircon grain. The youngest reproducible zircon from all six samples yield a weighted average $^{207}Pb/^{206}Pb$ age at 1836 ± 15 Ma (MSWD = 1.3; n = 6). Detrital zircon numbers refer to their analytical ID in the supplementary material Table 1.

Figure 8

Density distribution function for concordant and near-concordant (equal to or less than 5% discordance) $^{207}Pb/^{206}Pb$ ages (Ma). Modes in the age profile were estimated based on the cumulative age distribution from all six samples (vertical lines). The prominent mode at 1861 Ma likely reflects a mixture of locally derived detritus from the Wasekwan Group and intrusive suites (Pool Lake and Wathaman suites). Older detrital zircons require more distal zircon transport, possibly from the neighbouring cratons that border the THO. The maximum depositional age for the Sickle Group (1836 ± 15 Ma) is based on the youngest detrital zircon from all six samples.

Figure 9

Re-Os model age results for arsenopyrite and pyrite from the MacLellan, Gordon and Burnt Timber deposits. The most robust estimates for the timing of sulphidation in the LLGB are based on reproducible model ages for two highly-radiogenic arsenopyrite samples from the MacLellan deposit (i.e., 1824 and 1782 Ma). Model ages for the other moderately radiogenic mineral separates with a greater proportion of common Os are minimum ages and may not reflect the timing of hydrothermal fluids. The clustering of

Meso- and Neoproterozoic Re-Os model ages for some samples is of uncertain geological significance. These anomalously young ages could be geologically meaningless or reflect resetting during much younger reactivation of the THO.

Figure 10

Sulphide Pb isotope and trace element results for the MacLellan, Gordon, Burnt Timber gold deposits and one ore sample from the Lynn Lake Ni mine. Initial Pb isotope compositions were calculated based on an assumed age of 1.8 Ga, which is partially supported by Re-Os dating of the same mineral separate suite. With the exception of two anomalous samples, MacLellan and Burt Timber sulphide separates tend to yield more primitive initial Pb isotope composition compared to late-stage pyrite and pyrrhotite replacement ore zones at Gordon. Radiogenic mineral separates tend to be more Bi- and Te-rich despite significant scatter. Part of the scatter is likely related to precious metal-rich minerals that were included with arsenopyrite and pyrite during sample preparation. Incomplete homogenization of these mineral phases during pellet making provide a possible explanation for the elevated concentrations of these elements for some samples.

Figure 11

Compilation of previously reported and new ages for the Lynn Lake greenstone belt. Volcanic and plutonic U-Pb ages are from Baldwin et al. (1987), Turek et al. (2000), Beaumont-Smith and Böhm (2004, 2002), Beaumont-Smith et al. (2006), and Lawley et al. (2019). The inferred peak metamorphic age is based on metamorphic zircon results reported in Beaumont-Smith and Böhm (2004, 2002). The scatter of syenite and carbonatite ages are from Elliott (2009) and may reflect a combination of crystallization ages, metamorphic resetting, and/or isotopic disturbance. Sickle Group (U-Pb detrital zircon maximum depositional age) and hydrothermal/metamorphic ages (Re-Os sulphide and preliminary U-Pb monazite and xenotime results) were collected as part of the current study and Lawley et al. (2019). Biotite cooling ages are from O'Connor et al. (2019).

Figure 12

Cartoon showing basin development and inversion [basin geometry is schematic and adapted from (Scisciani et al., 2014)]. Deep-water sediments of the Kisseynew Basin (KB) were deposited in a back-arc during a synorogenic phase of extension at 1.85–1.84 Ga (Ansdell et al., 1995; Zwanzig and Bailes, 2010). Structural inversion of the back-arc was coeval with late-stage, arc-like granitic plutons and deposition of the fluvial/alluvial Sickle Group (1.84–1.83 Ga). In the Abitibi greenstone belt (Ontario-Quebec), Timiskaming-type basins and their extensional fault systems focus younger auriferous fluids from deep sources and preserve orogenic gold deposits in their structural footwall during inversion (Bleeker, 2012, 2015). Terminal collision involving the Hearne craton, intraoceanic arc complexes, and Sask and Superior cratons was coeval with peak metamorphism and steepening and folding of the inverted basin structural architecture. The earliest generation of auriferous fluids immediately post-date the syn-orogenic extensional phase, but are coeval with syenite and some late-stage dykes (tonalite and pegmatite).

References

Anderson, S., Böhm, C., 2001. Structural analysis and investigations of shear-hosted gold mineralization in the southern Lynn Lake greenstone belt (Parts of NTS 64C/11, /12, /15, /16). Rep. Act. 2001, Manitoba Ind. Trade Mines, Manitoba Geol. Surv. 67–75.

Ansdell, K., Connors, K., Stern, A., Lucas, S., 1999. Coeval sedimentation, magmatism, and fold-thrust development in the Trans-Hudson Orogen: Propagation of deformation into an active continental arc setting, Wekusko Lake area, Manitoba. Can. J. Earth Sci. 36, 275–291. doi:10.1139/e98-090

Ansdell, K., Norman, A., 1995. U-Pb geochronology and tectonic development of the southern flank of the Kisseynew Domain, Trans-Hudson Orogen, Canada. Precambrian Res. 72, 147–167.

Ansdell, K.M., 2005. Tectonic evolution of the Manitoba–Saskatchewan segment of the Paleoproterozoic Trans-Hudson. Can. J. Earth Sci. 759, 741–759. doi:10.1139/E05-035

Ansdell, K.M., Kyser, T.K., Stauffer, M.R., Edwards, G., 1992. Age and source of detrital zircons from the Missi Formation: a Proterozoic molasse deposit, Trans-Hudson Orogen, Canada. Can. J. Earth Sci. 29, 2583–2594. doi:10.1139/e92-205

Ansdell, K.M., Sciences, G., Place, S., Sn, S., Lucas, S.B., Connors, K., Stern, R.A., 1995. Kisseynew metasedimentary gneiss belt, Trans-Hudson orogen (Canada): Back-arc origin and collisional inversion. Geology 1039–1043.

Arndt, N., Todt, W., 1994. Formation of 1.9-Ga-old Trans-Hudson continental crust: Pb isotopic data. Chem. Geol. 118, 9–26.

Arne, D., Bierlein, F., Morgan, J., Stein, H., 2001. Re-Os dating of sulfides associated with gold mineralization in central victoria, Australia. Econ. Geol. 96, 1455–1439.

Ashton, K.E., Heaman, L.M., Lewry, J.F., Hartlaub, R.P., Shi, R., 1999. Age and origin of the Jan Lake

Complex: A glimpse at the buried Archean craton of the Trans-Hudson Orogen. Can. J. Earth Sci. 36, 185–208. doi:10.1139/e98-038

Augsten, B.E.K., Thorpe, R.I., Harris, D.C., Street, B., Ea, O.K.I.A., Fedikow, M.A.F., 1986. Ore mineralogy of the Aggasiz (MacLellan) gold deposit in the Lynn Lake region, Manitoba. Can. Mineral. 377, 369–377.

Bailes, A.H., 1980. Origin of early Proterozoic volcaniclastic turbidites, south margin of the Kisseynew sedimentary gneiss belt, File Lake, Manitoba. Precambrian Res. 12, 197–225. doi:10.1016/0301-9268(80)90029-7

Baldwin, D.A., Syme, E.C., Zwanzig, H. V, Gordon, T.M., Hunt, P.A., Stevens, R.D., 1987. U-Pb zircon ages from the Lynn Lake and Rusty Lake metavolcanic belts, Manitoba: two ages of Proterozoic magmatism. Can. J. Earth Sci. 24, 1053–1063.

Barley, M.E., Eisenlohr, B.N., Groves, D.I., Perring, C.S., Vearncombe, J.R., 1989. Late Archean convergent margin tectonics and gold mineralization: a new look at the Norseman-Wiluna Belt, Western Australia. Geology 17, 826–829. doi:10.1130/0091-7613(1989)017<0826:LACMTA>2.3.CO;2

Bateman, J., 1942. McVeigh Lake area, Manitoba. Geol. Surv. Canada, Pap. 45-14 34.

Beaumont-Smith, C., 2008. Geochemistry data for the Lynn Lake greenstone belt, Manitoba (NTS 64C11–16). Manitoba Sci. Technol. Energy Mines, Manitoba Geol. Surv. Open File OF2007-1 5.

Beaumont-Smith, C., 2003. Controls on gold mineralization associated with the Johnson shear zone and Agassiz metallotect, Lynn Lake greenstone belt: Summary of current activities (Parts of NTS 64C/10, /11, /12, /14, /15, /16). Rep. Act. 2000, Manitoba Ind. Trade Mines, Manitoba Geol. Surv. 49–50.

Beaumont-Smith, C., 2000. Structural analysis of the Johnson shear zone in the Gemmell Lake-Dunphy lakes area, Lynn Lake greenstone belt (PARTS OF NTS 64C/11, /12). Rep. Act. 2000, Manitoba Ind. Trade Mines, Manitoba Geol. Surv. 57–63.

Beaumont-Smith, C., Böhm, C., 2004. Structural analysis of the Lynn Lake greenstone belt (NTS 64C10, 11, 12, 14, 15 and 16). Rep. Act. 2004, Manitoba Ind. Econ. Dev. Mines, Manitoba Geol. Surv. 55–68.

Beaumont-Smith, C., Böhm, C., 2003. Tectonic evolution and gold metallogeny of the Lynn Lake greenstone belt, Manitoba (NTS 64C10, 11, 12, 14, 15 and 16). Rep. Act. 2003, Manitoba Ind. Trade Mines, Manitoba Geol. Surv. 39–49.

Beaumont-Smith, C., Böhm, C., 2002. Structural analysis and geochronological studies in the Lynn Lake greenstone belt and its gold-bearing shear zones (NTS 64C10, 11, 12, 14, 15 and 16), Manitoba. Rep. Act. 2002, Manitoba Ind. Trade Mines, Manitoba Geol. Surv. 159–170.

Beaumont-Smith, C., Lentz, D., Tweed, E., 2000. Structural analysis and gold metallogeny of the Farley Lake gold deposit, Lynn Lake greensotne belt. Rep. Act. 2000, Manitoba Ind. Trade Mines, Manitoba Geol. Surv. 73–81.

Beaumont-Smith, C., Machado, N., Peck, D., 2006. New uranium-lead geochronology results from the Lynn Lake greenstone belt, Manitoba (NTS 64C11–16). Manitoba Sci. Technol. Energy Mines, Manitoba Geol. Surv. Geosci. Pap. GP2006-1 11.

Bickford, M., Mock, T., Steinhart III, W., Collerson, K., Lewry, J., 2005. Origin of the Archean Sask craton and its extent within the Trans-Hudson orogen: evidence from Pb and Nd isotopic compositions of basement rocks and post-orogenic intrusions. Can. J. Earth Sci. 42, 659–684. doi:10.1139/E04-064

Bickford, M.E., Collerson, K.D., Sciences, E., Cruz, S., Lewry, J.F., Schmus, W.R. Van, Chiarenzelli, J.R., 1990. Proterozoic collisional tectonism in the Trans-Hudson orogen, Saskatchewan 14–18.

Bleeker, W., 2015. Synorogenic gold mineralization in granite-greenstone terranes: the deep connection between extension, major faults, synorogenic clastic basins, magmatism, thrust inversion, and long-term preservation, in: Dubé, B., Mercier-Langevin, P. (Eds.), Targeted Geoscience Initiative 4: Contributions to the Understanding of Precambrian Lode Gold Deposits and Implications for Exploration. pp. 25–47.

Bleeker, W., 2012. Lode gold deposits in ancient deformed and metamorphosed terranes: The role of extension in the formation of Timiskaming basins and large gold deposits, Abitibi Greenstone Belt — A discussion. Summ. F. Work Other Act. 2012, Ontario Geol. Surv. Open File Rep. 6280 1–12.

Cameron, E.M., 1993. Precambrian gold: perspectives from the top and bottom of shear zones. Can. Mineral. 31, 917–944.

Cawood, P., Kröner, A., Collins, W., Kusky, T., Mooney, W., Windley, B., 2009. Accretionary orogens through Earth history, in: Cawood, P., Kröner, A. (Eds.), Earth Accretionary Systems in Space and Time. Geological Society, London, Special Publications, 318, pp. 1–36.

Cawood, P.A., Hawkesworth, C.J., Dhuime, B., 2012. Detrital zircon record and tectonic setting. Geology 40, 875–878. doi:10.1130/G32945.1

Chakhmouradian, A., Couëslan, C., Reguir, E., 2009. Evidence for carbonatite magmatism at Paint Lake , Manitoba (parts of NTS 63O8 , 63P5, 12). Rep. Act. 2009, Manitoba Innov. Energy Mines, Manitoba Geol. Surv. 118–126.

Chakhmouradian, A.R., Mumin, A.H., Demény, A., Elliott, B., 2008. Postorogenic carbonatites at Eden Lake, Trans-Hudson Orogen (northern Manitoba, Canada): Geological setting, mineralogy and geochemistry. Lithos 103, 503–526. doi:10.1016/j.lithos.2007.11.004

Connors, K.A., Ansdell, K.M., Lucas, S.B., 1999. Coeval sedimentation, magmatism, and fold–thrust development in the Trans-Hudson Orogen: propagation of deformation into an active continental arc setting, Wekusko Lake. Can. J. Earth Sci. 291, 275–291.

Corfu, F., Jackson, S.L., Sutcliffe, R.H., 1991. U-Pb ages and tectonic significance of late Archean alkalic magmatism and nonmarine sedimentation: Timiskaming Group, southern Abitibi Belt, Ontario. Can. J. Earth Sci. 28, 489–503. doi:10.1139/e91-043

Corrigan, D., Hajnal, Z., Németh, B., Lucas, S.B., 2005. Tectonic framework of a Paleoproterozoic arc–continent to continent–continent collisional zone, Trans-Hudson Orogen, from geological and seismic reflection studies. Can. J. Earth Sci. 434, 421–434. doi:10.1139/E05-025

Corrigan, D., Maxeiner, R., Harper, C., 2001. Preliminary U-Pb results from the La Ronge-Lynn Lake bridge project. Summ. Investig. 2001, Vol. 2, Saskatchewan Geol. Surv. Saskatchewan Energy Mines, Misc. Report, 2001-4.2. 5.

Corrigan, D., Pehrsson, S., Wodicka, N., de Kemp, E., 2009. The Palaeoproterozoic Trans-Hudson Orogen: a prototype of modern accretionary processes. Geol. Soc. London, Spec. Publ. 327, 457–479. doi:10.1144/SP327.19

Couëslan, C.G., Pattison, D.R.M., Dufrane, S.A., 2013. Paleoproterozoic metamorphic and deformation history of the Thompson Nickel Belt, Superior Boundary Zone, Canada, from in situ U–Pb analysis of monazite. Precambrian Res. 237, 13–35. doi:10.1016/j.precamres.2013.06.009

Cousens, B., 1996. Magmatic evolution of Quaternary mafic magmas at Long Valley Caldera and the Devils Postpile, California: Effects of crustal contamination on lithospheric mantle-derived magmas. J. Geophys. Res. 101, 27673–27889.

Cousens, B.L., Aspler, L.B., Chiarenzelli, J.R., Donaldson, J.A., Sandeman, H., Peterson, T.D., LeCheminant, A.N., 2002. Enriched Archean lithospheric mantle beneath western Churchill Province tapped during Paleoproterozoic orogenesis. Geology 29, 827–830. doi:10.1130/0091-7613(2001)029<0827:EALMBW>2.0.CO;2

David, J., Bailes, A.H., Machado, N., 1996. Evolution of the Snow Lake portion of the Palaeoproterozoic Flin Flon and Kisseynew belts, Trans-Hudson Orogen, Manitoba, Canada. Precambrian Res. 80, 107–124. doi:10.1016/s0301-9268(96)00008-3

Davis, W., Pestaj, T., Rayner, N., McNicoll, V., 2019. Long-term reproducibility of 207Pb/206Pb age at the GSC SHRIMP lab based on the GSC Archean Reference Zircon z1242. Geol. Surv. Canada, Sci. Present. 111.

De Souza, S., Dubé, B., Mercier-Langevin, P., McNicoll, V., Dupuis, C., Kjarsgaard, I., 2019. Hydrothermal alteration mineralogy and geochemistry of the Archean world-class Canadian malartic disseminated-stockwork gold deposit, southern Abitibi Greenstone Belt, Quebec, Canada. Econ. Geol. 114, 1057–1094. doi:10.5382/econgeo.4674

Dubé, B., Gosselin, P., 2007. Greenstone-hosted quartz-carbonate vein deposits, in: Mineral Deposits of Canada: A Synthesis of Major Deposit-Types, District Metallogeny, the Evolution of Geological Provinces, and Exploration Methods. pp. 49–74.
Eckstrand, R., Hulbert, L., 2007. Magmatic nickel-copper-platinum group element deposits, in: Mineral Deposits of Canada: A Synthesis of Major Deposit-Types, District Metallogeny, the Evolution of Geological Provinces, and Exploration Methods. Geological Association of Canada, pp. 205–222.
Elliott-Meadows, S., Froese, E., Appleyard, E., 2000. Cordierite-anthophyllite-cummingtonite rocks from the Lar Deposit, Laurie Lake, Manitoba. Can. Mineral. 38, 545–550.
Elliott, B.R., 2009. A mineralogical, geochemical and geochronological study of postorogenic carbonatites in the Eden Lake complex, northern Manitoba. University of Manitoba.
Faure, S., 2010. World Kimberlites CONSOREM Database (Version 3). Consort. Rech. en Explor. Minérale CONSOREM, Univ. du Québec à Montréal.
Fedikow, M., Gale, G., 1982. Mineral deposit studies in the Lynn Lake area. Manitoba Dep. Energy Mines, Rep. F. Stud. 44–54.
Fumerton, S.L., Stauffer, M.R., Lewry, J.F., 1984. The Wathaman batholith: largest known Precambrian pluton. Can. J. Earth Sci. 21, 1082–1097. doi:10.1139/e84-113
Galley, A., Hannington, M., Jonasson, I., 2007. Volcanogenic massive sulphide deposits, in: Mineral Deposits of Canada: A Synthesis of Major Deposit-Types, District Metallogeny, the Evolution of Geological Provinces, and Exploration Methods. pp. 141–162.
Gilbert, H., Syme, E., Zwanzig, H., 1980. Geology of the metavolcanic and volcaniclastic metasedimentary rocks in the Lynn Lake area. Manitoba Energy Mines, Geol. Serv. GP80-1 118.
Glendenning, M.W.P., Gagnon, J.E., Polat, A., 2014. Geochemistry of the metavolcanic rocks in the vicinity of the MacLellan Au-Ag deposit and an evaluation of the tectonic setting of the Lynn Lake greenstone belt, Canada: Evidence for a Paleoproterozoic-aged rifted continental margin. Lithos 233, 46–68. doi:10.1016/j.lithos.2015.05.022
Goldfarb, R.J., Groves, D.I., Gardoll, S., 2001. Orogenic gold and geologic time: a global synthesis. Ore Geol. Rev. 18, 1–75.
Gordon, T., Hunt, P., Bailes, A., Syme, E., 1990. U-Pb zircon ages from the Flin Flon and Kisseynew belt, Manitoba: chronology of crust formation at an Early Proterozoic accretionary margin, in: Lewry, J., Stauffer, M. (Eds.), The Early Proterozoic Trans-Hudson Orogen of North America. Geological Association of Canada, Special Paper 37, pp. 177–199.
Griffin, W., Powell, W., Pearson, N., O'Reilly, S., 2008. GLITTER: Data reduction software for laser ablation ICP-MS. Mineralogical Association of Canada Short Course Series, pp. 308–311.
Groves, D., Goldfarb, R., Gebre-Mariam, M., Hagemann, S., Robert, F., 1998. Orogenic gold deposits: A proposed classification in the context of their crustal distribution and relationship to other gold deposit types. Ore Geol. Rev. 13, 7–27.
Hastie, E.C.G., Gagnon, J.E., Samson, I.M., Lake, L., 2018. The Paleoproterozoic MacLellan deposit and related Au-Ag occurrences, Lynn Lake greenstone belt, Manitoba: An emerging, structurally-controlled gold camp. Ore Geol. Rev. 94, 24–45. doi:10.1016/j.oregeorev.2018.01.016
Hoffman, P., 1988. United plates of america, the birth of a craton: Early Proterozoic assembly and growth of Laurentia. Annu. Rev. Earth Planet. Sci. 16, 543–603.
Hollings, P., Ansdell, K., 2002. Paleoproterozoic arc magmatism imposed on an older backarc basin: Implications for the tectonic evolution of the Trans-Hudson orogen, Canada. Geol. Soc. Am. Bull. 114, 153–168.
Hyde, R.S., 1980. Sedimentary facies in the Archean Timiskaming Group and their tectonic implications, Abitibi greenstone belt, northeastern Ontario, Canada. Precambrian Res. 12, 161–195.
Jochum, K.P., Nohl, U., Herwig, K., Lammel, E., Stoll, B., Hofmann, A.W., 2005. GeoReM: A new geochemical database for reference materials and isotopic standards. Geostand. Geoanalytical Res. 29, 333–338.
Jones, L., Beaumont-Smith, C., Lafrance, B., 2000. Preliminary structural and gold metallogenic studies at the Burnt Timber mine and surrounding area, Lynn Lake greenstone belt (NTS 64C/10). Rep. Act.

2000, Manitoba Ind. Trade Mines, Manitoba Geol. Surv. 69–72.
Jones, L., Lafrance, B., Beaumont-Smith, C., 2006. Structural controls on gold mineralization at the Burnt Timber mine, Lynn Lake greenstone, Trans-Hudson orogen, Manitoba. Explor. Min. Geol. 15, 89–100.
Kendall, B., Creaser, R.A., Gordon, G.W., Anbar, A.D., 2009. Re-Os and Mo isotope systematics of black shales from the Middle Proterozoic Velkerri and Wollogorang Formations, McArthur Basin, northern Australia. Geochim. Cosmochim. Acta 73, 2534–2558. doi:10.1016/j.gca.2009.02.013
Kerrich, R., Wyman, D., 1990. Geodynamic setting of mesothermal gold deposits: An association with accretionary tectonic regimes. Geology 18, 882–885.
Krapež, B., Barley, M.E., 2008. Late Archaean synorogenic basins of the Eastern Goldfields Superterrane, Yilgarn Craton, Western Australia. Part III. Signatures of tectonic escape in an arc-continent collision zone. Precambrian Res. 161, 183–199. doi:10.1016/j.precamres.2007.06.020
Kraus, J., Menard, T., 1997. A thermal gradient at constant pressure: Implications for low- to medium-pressure metamorphism in a compressional tecotnic setting, Flin Flon and Kisseynew domains, Trans-Hudson, Orogen, Central Canada. Can. Mineral. 35, 1117–1136.
Lawley, C., Creaser, R. a., Jackson, S.E., Yang, Z., Davis, B., Pehrsson, S., Dubé, B., Mercier-Langevin, P., Vaillancourt, D., 2015. Unravelling the western Churchill Province Paleoproterozoic gold metallotect: Constraints from Re-Os arsenopyrite and U-Pb xenotime geochronology and LA-ICPMS arsenopyrite trace element chemistry at the BIF-hosted Meliadine Gold District, Nunavut, Canada. Econ. Geol. 1425–1454.
Lawley, C., Davis, W., Jackson, S., Petts, D., Yang, E., Zhang, S., Selby, D., O'Connor, A., Schneider, D., 2019. Paleoproterozoic gold and its tectonic triggers and traps, in: Rogers, N. (Ed.), Targeted Geoscience Initiative: 2018 Report of Activities. Geological Survey of Canada, Open File.
Lawley, C., Jackson, S., Yang, Z., Davis, W., Eglington, B., 2017. Tracing the transition of gold from source to sponge to sink. Econ. Geol. 112, 169–183.
Lawley, C., Pearson, D., Waterton, P., Zagorevski, A., Bédard, J., Jackson, S., Petts, D., Kjarsgaard, B., Zhang, S., Wright, D., 2020. Element and isotopic signature of re-fertilized mantle peridotite as determined by nanopowder and olivine LA-ICPMS analyses. Chem. Geol. 536.
Lawley, C., Schneider, D., Yang, E., Davis, W., Jackson, S., Yang, Z., Zhang, S., Selby, D., 2018. Age relationships and preliminary U-Pb zircon geochronology results from the Lynn Lake Greenstone Belt, in: Rogers, N. (Ed.), 2017 Report of Activities, Geological Survey of Canada, Open File 8358. pp. 133–137.
Lawley, C., Selby, D., Imber, J., 2013. Re-Os molybdenite, pyrite and chalcopyrite geochronology, Lupa Goldfield, SW Tanzania: Implications for metallogenic time scales and shear zone reactivation. Econ. Geol. 15, 1591–1613. doi:10.2113/econgeo.108.7.1591
Le Mignot, E., Reisberg, L., André-Mayer, A.S., Bourassa, Y., Fontaine, A., Miller, J., 2017. Re-Os geochronological evidence for multiple Paleoproterozoic gold events at the scale of the West African craton. Econ. Geol. 112, 145–168. doi:10.2113/econgeo.112.1.145
Lewry, J., 1983. Character and structural relations of the "Mclennan Group" meta-arkoses, McLennan-Jaysmlth lakes area. Summ. Investig. 1983, Saskatchewan Geol. Surv. Saskatchewan Energy Mines, Misc. Rep. 83-4 49–55. doi:10.1017/CBO9781107415324.004
Lewry, J., Hajnal, Z., Green, A., Lucas, S., White, D., Stauffer, M., Ashton, K., Weber, W., Clowes, R., 1994. Structure of a Paleoproterozoic continent-continent collision zone: a LITHOPROBE seismic reflection profile across the Trans-Hudson Orogen, Canada. Tecotnophysics 232, 143–160.
Lewry, J.F., 1981. Lower proterozoic arc-microcontinent collisional tectonics in the western Churchill Province. Nature 294, 69–72. doi:10.1038/294069a0
Lowdon, J., Stockwell, C., Tipper, H., Wanless, R., 1963. Age determinations and geological studies. Geol. Surv. Canada, Pap. 62-17 140.
Ludwig, K., 2009. Squid 2: A user's manual. Berkeley Geochronol. Cent. 5, 110.
Ma, G., Beaumont-Smith, C., 2001. Stratigraphic and structural mapping of the Agassiz metallotect near Lynn Lake, Lynn Lake greenstone belt (parts of NTS 64C/14, /15). Rep. Act. 2001, Manitoba Ind.

Trade Mines, Manitoba Geol. Surv. 86–93.
Ma, G., Beaumont-Smith, C., Lentz, D., 2000. Preliminary structural analysis of the Agassiz Metallotect near the MacLellan and Dot Lake gold deposits, Lynn Lake greenstone belt (parts of NTS 64C/14, /15); Rep. Act. 2000, Manitoba Ind. Trade Mines, Manitoba Geol. Surv. 51–56.
Machado, N., Gapais, D., Potrel, A., Gauthier, G., Hallot, E., 2011. Chronology of transpression, magmatism, and sedimentation in the Thompson Nickel Belt (Manitoba, Canada) and timing of Trans-Hudson Orogen - Superior Province collision. Can. J. Earth Sci. 48, 295–324. doi:10.1139/E10-040
Machado, N., Zwanzig, H., Parent, M., 1999. U–Pb ages of plutonism, sedimentation, and metamorphism of the Paleoproterozoic Kisseynew metasedimentary belt, Trans-Hudson Orogen (Manitoba, Canada). Can. J. Earth Sci. 1842, 1829–1842.
Martins, T., Couëslan, C.G., Böhm, C.O., 2012. Rare metals scoping study of the Brezden Lake intrusive complex, western Manitoba (part of NTS 64C4). Rep. Act. 2012, Manitoba Innov. Energy Mines, Manitoba Geol. Surv. 115–123.
Martins, T., Couëslan, C.G., Böhm, C.O., 2011. The Burntwood Lake alkali-feldspar syenite revisited, west-central Manitoba (part of NTS 63N8). Rep. Act. 2011, Manitoba Innov. Energy Mines, Manitoba Geo- Log. Surv. 79–85.
Maxeiner, R., 1999. La Ronge-Lynn Lake Bridge: Geology of the Wapus Bay-Lowdermilk Bay (Reindeer Lake) Area. Summ. Investig. 1999, Vol. 2, Saskatchewan Geol. Surv. Saskatchewan Energy Mines, Misc. Rep. 99-4.2 143–158.
Maxeiner, R., Demmans, C., 2000. The final pieces of the "Bridge": Geology of the Southern Reindeer lake and Laurie lake areas. Summ. Investig. 2000, Vol. 2. Saskatchewan Geol. Surv. Sask. Energy Mines. Misc. Rep. 2000-4.2 30–50.
Maxeiner, R.O., Corrigan, D., Harper, C.T., Macdougall, D.G., Ansdell, K., 2005. Paleoproterozoic arc and ophiolitic rocks on the northwest-margin of the Trans-Hudson Orogen, Saskatchewan, Canada: their contribution to a revised tectonic framework for the orogen. Precambrian Res. 136, 67–106. doi:10.1016/j.precamres.2004.10.003
Maxeiner, R.O., Kamber, B.S., 2011. La Ronge "Horseshoe" project: Bedrock Geology of the Hebden Lake Area at the Transition Between the Western Glennie Domain and Southern Kisseynew and La Ronge Domains (parts of NTS 73P/07). Summ. Investig. 2011, Vol. 2, Saskatchewan Geol. Surv. Sask. Minist. Energy Resour. Misc. Rep. 2011-4.2, Pap. A-7 20.
Maxeiner, R.O., Morelli, R., 2014. The Mullock Lake Assemblage: Remnants of an 1846 to 1837 Ma Forearc Basin ? Summ. Investig. 2014, Vol. 2, Saskatchewan Geol. Surv. Sask. Minist. Econ. Misc. Rep. 2014-4.2, Pap. A-7 14. doi:10.13140/RG.2.2.11973.96488
Maxeiner, R.O., Rayner, N., 2011. Continental arc magmatism along the southeast Hearne Craton margin in Saskatchewan, Canada: Comparison of the 1.92-1.91Ga Porter Bay Complex and the 1.86-1.85Ga Wathaman Batholith. Precambrian Res. 184, 93–120. doi:10.1016/j.precamres.2010.10.005
McDannell, K.T., Zeitler, P.K., Schneider, D.A., 2018. Instability of the southern Canadian Shield during the late Proterozoic. Earth Planet. Sci. Lett. 490, 100–109. doi:10.1016/j.epsl.2018.03.012
Meyer, M., Bickford, M., Lewry, J., 1992. The Wathaman batholith: An Early Proterozoic continental arc in the Trans-Hudson orogenic belt, Canada. Geol. Soc. Am. Bull. 104, 1073–1085.
Milligan, G., 1960. Geology of the Lynn Lake district. Manitoba Dep. Mines Nat. Resour. Mines Branch, Publ. 57-1 317.
Moore, J., Hart, S., Barnett, C., Hurley, P., 1960. Potassium-argon ages in Northern Manitoba. Bull. Geol. Soc. Am. 71, 225.
Morelli, R.M., Creaser, R.A., Selby, D., Kontak, D.J., Horne, R.J., 2005. Rhenium-osmium geochronology of arsenopyrite in Meguma group gold deposits, Meguma terrane, Nova Scotia, Canada: Evidence for multiple gold-mineralizing events. Econ. Geol. 100, 1229–1242. doi:10.2113/gsecongeo.100.6.1229
Mueller, W., Donaldson, J.A., 1992. Development of sedimentary basins in the Archean Abitibi Belt, Canada: an overview. Can. J. Earth Sci. 29, 2249–2265. doi:10.1139/e92-177

Mumin, A.H., Corriveau, L., 2004. Eden deformation corridor and polymetallic mineral belt, Trans-Hudson Orogen, Leaf Rapids area, Manitoba (NTS 64B and 64C). Rep. Act. 2004, Manitoba Ind. Econ. Dev. ment Mines, Manitoba Geol. Surv. 69–91.

Norman, G., 1934. Granville Lake district, northern Manitoba. Geol. Surv. Canada, Summ. Report, 1934, Pt. C, 23–41.

O'Connor, R., Lawley, C., Schneider, D., 2019. Linking metamorphism and orogenic gold in the Proterozoic Lynn Lake greenstone belt, northern Manitoba, in: GAC-MAC-IAH: Where Geosciences Converge. The Geological Association of Canada, Quebec City, p. 153.

Park, A.F., Lentz, D.R., 2002. Structure and Stratigraphy in the Agassiz Metallotect, Lynn Lake Greenstone Belt (NTS 64C14 and 64C15), Manitoba 171–186.

Peck, D., Lin, S., Atkin, K., Eastwood, A., 1998. Reconnaissance structural studies of Au metallotects in the Lynn Lake greenstone belt (Parts of NTS 64C/10, C/11, C/15). Manitoba Energy Mines, Geol. Serv. Rep. Act. 69–74.

Poulsen, K.H., Card, K.D., Franklin, J.M., 1992. Archean tectonic and metallogenic evolution of the superior province of the canadian shield. Precambrian Res. 58, 25–54. doi:10.1016/0301-9268(92)90111-Z

Rasmussen, B., Sheppard, S., Fletcher, I.R., 2006. Testing ore deposit models using in situ U-Pb geochronology of hydrothermal monazite: Paleoproterozoic gold mineralization in northern Australia. Geology 34, 77–80. doi:10.1130/G22058.1

Rubatto, D., 2002. Zircon trace element geochemistry: partitioning with garnet and the link between U–Pb ages and metamorphism. Chem. Geol. 184, 123–138.

Samson, I., Gagnon, J., 1995. Episodic fluid infiltration and genesis of the Proterozoic MacLellan Au-Ag deposit, Lynn Lake greenstone belt. Explor. Min. Geol. 4, 33–50.

Samson, I.M., Blackburn, W.H., Gagnon, J.E., 1999. Paragenesis and composition of amphibole and biotite in the MacLellan gold deposit, Lynn Lake greenstone belt, Manitoba, Canada. Can. Mineral. 37, 1405–1421.

Sangster, D.F., 1978. Isotopic studies of ore-leads of the circum-Kisseynew volcanic belt of Manitoba and Saskatchewan. Can. J. Earth Sci. 15, 1112–1121.

Schneider, D.A., Heizler, M.T., Bickford, M.E., Wortman, G.L., Condie, K.C., Perilli, S., 2007. Timing constraints of orogeny to cratonization: Thermochronology of the Paleoproterozoic Trans-Hudson orogen, Manitoba and Saskatchewan, Canada. Precambrian Res. 153, 65–95. doi:10.1016/j.precamres.2006.11.007

Scisciani, V., Agostini, S., Calamita, F., Pace, P., Cilli, A., Giori, I., Paltrinieri, W., 2014. Positive inversion tectonics in foreland fold-and-thrust belts: A reappraisal of the Umbria-Marche Northern Apennines (Central Italy) by integrating geological and geophysical data. Tectonophysics 637, 218–237. doi:10.1016/j.tecto.2014.10.010

Selby, D., Kelley, K., Hitzman, M., Zieg, J., 2009. Re-Os sulfide (bornite, chalcopyrite, and pyrite) systematics of the carbonate-hosted copper deposits at Ruby Creek, southern Brooks Range, Alaska. Econ. Geol. 104, 437–444.

Shirey, S.B., Walker, R.J., 1995. Carius tube digestion for low-blank rhenium-osmium analysis. Anal. Chem. 67, 2136–2141. doi:10.1021/ac00109a036

Smoliar, M., Walker, R., Morgan, J., 1996. Re-Os ages of group IIA , IIIA, IVA, and IVB iron meteorites. Science (80-.). 271, 1099–1102.

Stacey, J.S., Kramers, J.D., 1975. Approximation of terrestrial lead isotope evolution by a two-stage model. Earth Planet. Sci. Lett. 26, 207–221. doi:10.1016/0012-821X(75)90088-6

Staples, P., Mclean, E., Volk, J., Toscano, P., Cobbina, A., Besemann, K., Castro, L., Couto, R., Koniaris, E., 2017. NI 43-101 technical report feasibility study for the Lynn Lake gold project, Manitoba, Canada.

Stauffer, M., 1984. Manikewan: An early Proterozoic ocean in central Canada, its igneous history and oroegnic closure. Precambrian Res. 25, 257–281.

Stein, H., Morgan, J., Scherstén, A., 2000. Re-Os dating of low-level highly radiogenic (LLHR) sulfides:

The Harnäs gold deposit, southwest Sweden, records continental-scale tectonic events. Econ. Geol. 95, 1657–1672. doi:10.2113/gsecongeo.95.8.1657
Stern, R.A., 1997. The GSC Sensitive High Resolution Ion Microprobe (SHRIMP): Analytical techniques of zircon U-Th-Pb age determinations and performance evaluation. Radiogenic Age Isot. Stud. Rep. 10; Geol. Surv. Canada, Curr. Res. 1997-F 1–31.
Syme, E., 1988. Athapapuskow Lake project. Manitoba Energy Mines Rep. Act. 20–34.
Syme, E., 1985. Geochemistry of metavolcanic rock in the Lynn Lake belt. Manitoba Energy Mines, Geol. Serv. 84.
Symons, D.T.A., Harris, M.J., 2005. Accretion history of the Trans-Hudson Orogen in Manitoba and Saskatchewan from paleomagnetism. Can. J. Earth Sci. 42, 723–740. doi:10.1139/e04-090
Todt, W., Cliff, R., Hofmann, A., 1996. Evaluation of a 202Pb-205Pb double spike for high-precision lead isotope analysis, in: Earth Processes: Reading the Isotopic Code. American Geophysical Union.
Turek, A., 1967. Age of sulfide mineralization at Lynn Lake, Manitoba. Can. J. Earth Sci. 4, 572–574.
Turek, A., Woodhead, J., Zwanzig, H., 2000. U-Pb Age of the gabbro and other plutons at Lynn Lake (Part of NTS 64C). Rep. Act. 2000, Manitoba Ind. Trade Mines, Manitoba Geol. Surv. 97–104.
Whalen, J.B., Syme, E.C., Stern, R.A., 1999. Geochemical and Nd isotopic evolution of Paleoproterozoic arc-type granitoid magmatism in the Flin Flon Belt, Trans-Hudson orogen, Canada. Can. J. Earth Sci. 36, 227–250. doi:10.1139/e98-026
White, D.J., 2005. High-temperature, low-pressure metamorphism in the Kisseynew domain, Trans-Hudson orogen: crustal anatexis due to tectonic thickening? Can. J. Earth Sci. 721, 707–721. doi:10.1139/E04-087
White, D.J., Zwanzig, H. V, Hajnal, Z., 2000. Crustal suture preserved in the Paleoproterozoic Trans-Hudson orogen, Canada. Geology 28, 527–530.
Wilson, J., 1966. Did the atlantic close and then reopen? Nature 211, 676–681. doi:10.12789/geocanj.2016.43.109
Woolley, A., Kjarsgaard, B., 2008. Carbonatite occurrences of the world: map and database. Geol. Surv. Canada, Open File 5796 28.
Yang, X., Lawley, C., 2018. Tectonic setting of the Gordon gold deposit, Lynn Lake greenstone belt, northwestern Manitoba (parts of NTS 64C16): evidence from lithogeochemistry, Nd isotopes and U-Pb geochronology. Rep. Act. 2018, Manitoba Growth, Enterp. Trade, Manitoba Geol. Surv. 89–109.
Zwanzig, H., 1997. Kisseynew metasedimentary gneiss belt, Trans-Hudson orogen (Canada): Back-arc origin and collisional inversion: Comment and Reply. Geology 1995–1997.
Zwanzig, H., Bailes, A., 2010. Geology and geochemical evolution of the northern Flin Flon and southern Kisseynew domains, Kississing–File lakes area, Manitoba (parts of NTS 63K, N). Manitoba Innov. Energy Mines, Manitoba Geol. Surv. Geosci. Rep. GR2010-1 135.
Zwanzig, H., Syme, E., Gilbert, H., 1999. Updated trace element geochemistry of ca. 1.9 Ga metavolcanic rocks in the Paleoproterozoic Lynn Lake Belt. Manitoba Ind. Trade Mines, Geol. Serv. Open File Rep. 99-13 46.
Zwanzig, H. V, 1999. Structure and stratigraphy of the south flank of the Kisseynew Domain in the Trans-Hudson Orogen, Manitoba: implications for 1.845–1. 77 Ga collision tectonics. Can. J. Earth Sci. 1880, 1859–1880.
Zwanzig, H. V, Lake, L., Lake, L., 2008. Correlation of lithological assemblages flanking the Kisseynew Domain, Manitoba (parts of NTS 63N, 63O, 64B, 64C): proposal for tectonic / metallogenic subdomains. Rep. Act. 2008, Manitoba Sci. Technol. Energy Mines, Manitoba Geol. Surv. 38–52.

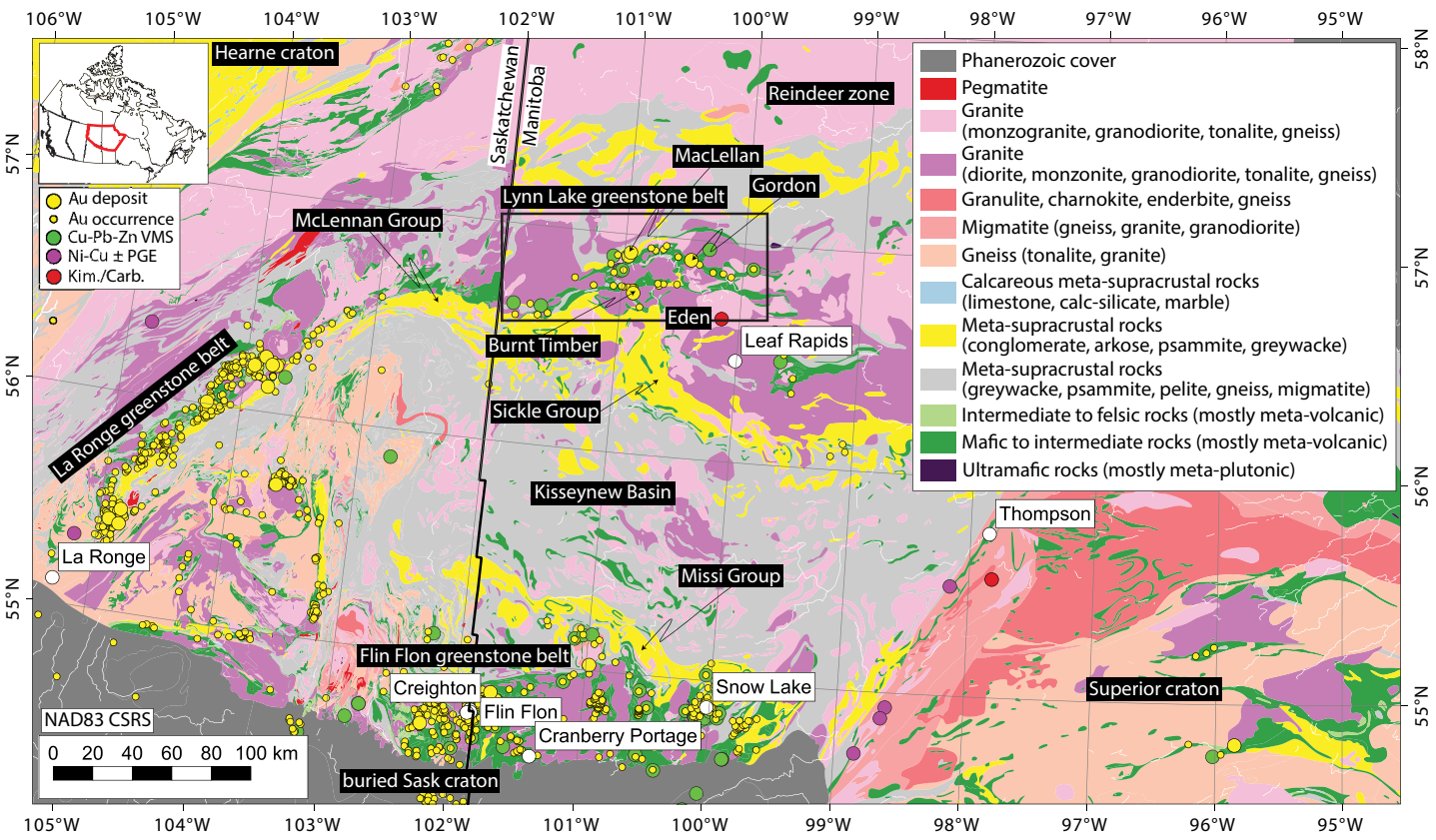
106°W
105°W
104°W
103°W
102°W
101°W
100°W
99°W
98°W
97°W
96°W
95°W
58°N
57°N
56°N
55°N
Hearne craton
Saskatchewan
Manitoba
Reindeer zone
MacLellan
Gordon
Lynn Lake greenstone belt
McLennan Group
Eden
Leaf Rapids
Burnt Timber
La Ronge greenstone belt
Sickle Group
Kisseynew Basin
Thompson
La Ronge
Missi Group
Flin Flon greenstone belt
Creighton
Flin Flon
Snow Lake
Cranberry Portage
Superior craton
buried Sask craton
NAD83 CSRS
0 20 40 60 80 100 km
Au deposit
Au occurrence
Cu-Pb-Zn VMS
Ni-Cu ± PGE
Kim./Carb.
Phanerozoic cover
Pegmatite
Granite (monzogranite, granodiorite, tonalite, gneiss)
Granite (diorite, monzonite, granodiorite, tonalite, gneiss)
Granulite, charnokite, enderbite, gneiss
Migmatite (gneiss, granite, granodiorite)
Gneiss (tonalite, granite)
Calcareous meta-supracrustal rocks (limestone, calc-silicate, marble)
Meta-supracrustal rocks (conglomerate, arkose, psammite, greywacke)
Meta-supracrustal rocks (greywacke, psammite, pelite, gneiss, migmatite)
Intermediate to felsic rocks (mostly meta-volcanic)
Mafic to intermediate rocks (mostly meta-volcanic)
Ultramafic rocks (mostly meta-plutonic)

Figure 1

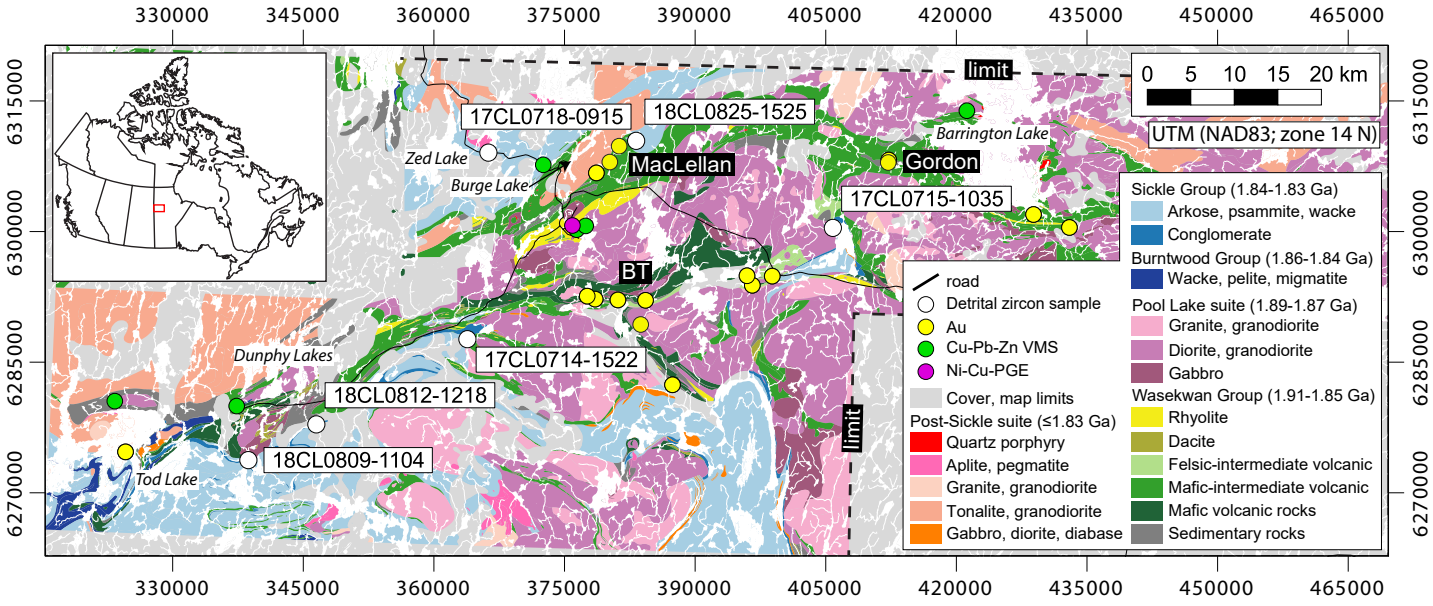
330000
345000
360000
375000
390000
405000
420000
435000
450000
465000
6315000
6300000
6285000
6270000
limit
0 5 10 15 20 km
UTM (NAD83; zone 14 N)
17CL0718-0915
18CL0825-1525
MacLellan
Zed Lake
Burge Lake
Barrington Lake
Gordon
17CL0715-1035
BT
17CL0714-1522
Dunphy Lakes
18CL0812-1218
18CL0809-1104
Tod Lake
road
Detrital zircon sample
Au
Cu-Pb-Zn VMS
Ni-Cu-PGE
Cover, map limits
Post-Sickle suite (≤1.83 Ga)
Quartz porphyry
Aplite, pegmatite
Granite, granodiorite
Tonalite, granodiorite
Gabbro, diorite, diabase
Sickle Group (1.84-1.83 Ga)
Arkose, psammite, wacke
Conglomerate
Burntwood Group (1.86-1.84 Ga)
Wacke, pelite, migmatite
Pool Lake suite (1.89-1.87 Ga)
Granite, granodiorite
Diorite, granodiorite
Gabbro
Wasekwan Group (1.91-1.85 Ga)
Rhyolite
Dacite
Felsic-intermediate volcanic
Mafic-intermediate volcanic
Mafic volcanic rocks
Sedimentary rocks

Figure 2

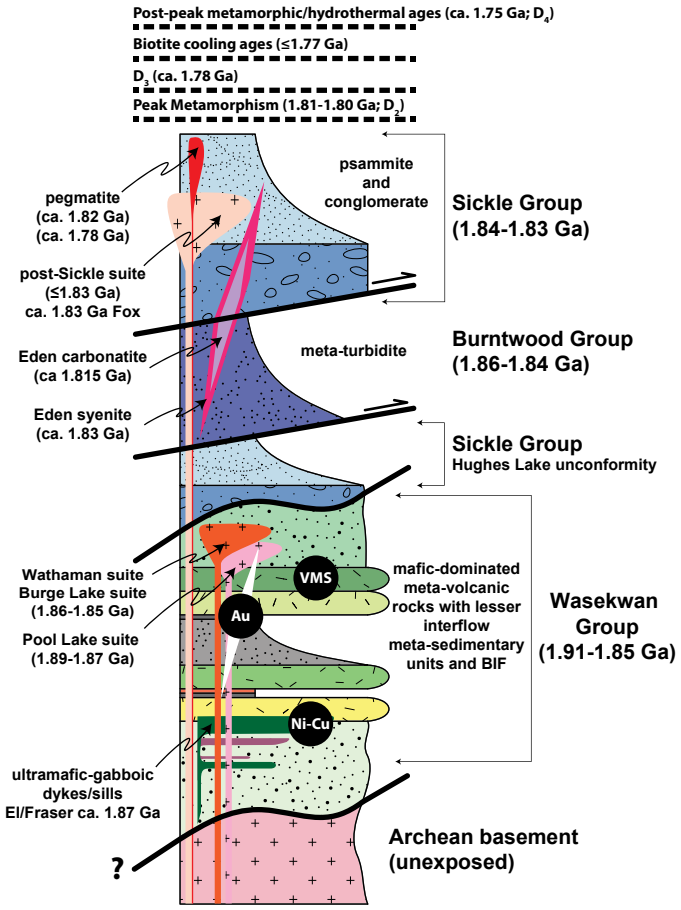
Post-peak metamorphic/hydrothermal ages (ca. 1.75 Ga; D4)
Biotite cooling ages (≤1.77 Ga)
D3 (ca. 1.78 Ga)
Peak Metamorphism (1.81-1.80 Ga; D2)
psammite and conglomerate
Sickle Group (1.84-1.83 Ga)
pegmatite (ca. 1.82 Ga) (ca. 1.78 Ga)
post-Sickle suite (≤1.83 Ga) ca. 1.83 Ga Fox
meta-turbidite
Burntwood Group (1.86-1.84 Ga)
Eden carbonatite (ca 1.815 Ga)
Eden syenite (ca. 1.83 Ga)
Sickle Group
Hughes Lake unconformity
Wathaman suite
Burge Lake suite (1.86-1.85 Ga)
Pool Lake suite (1.89-1.87 Ga)
VMS
Au
mafic-dominated meta-volcanic rocks with lesser interflow meta-sedimentary units and BIF
Wasekwan Group (1.91-1.85 Ga)
Ni-Cu
ultramafic-gabbroic dykes/sills
El/Fraser ca. 1.87 Ga
?
Archean basement (unexposed)

Figure 3

Rock photos of detrital zircon samples

Figure 4

Core photos of veins and hydrothermal alteration

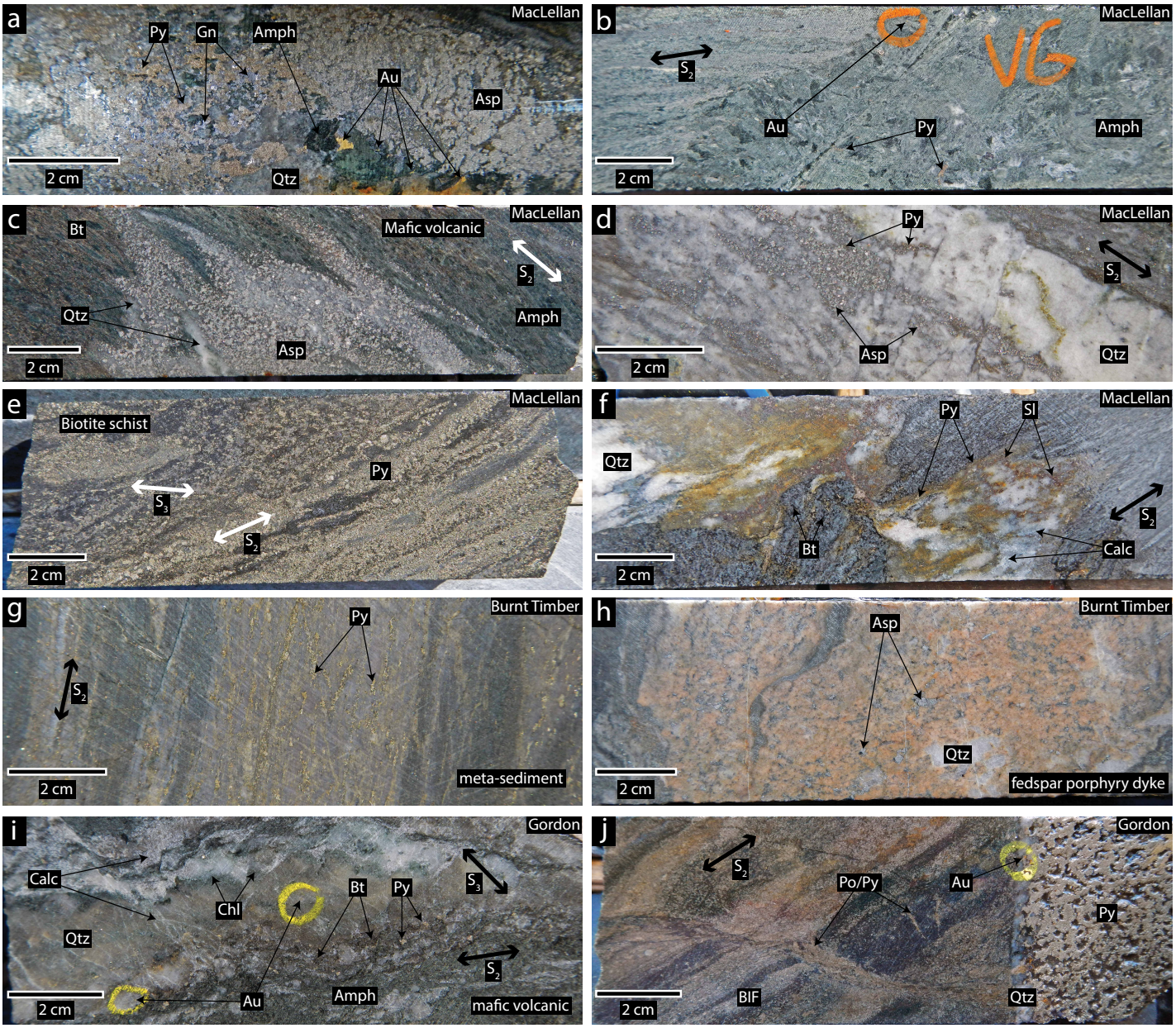

Figure 5

Scanning electron microscope (SEM) backscattered electron (BSE) images of gold ore zones

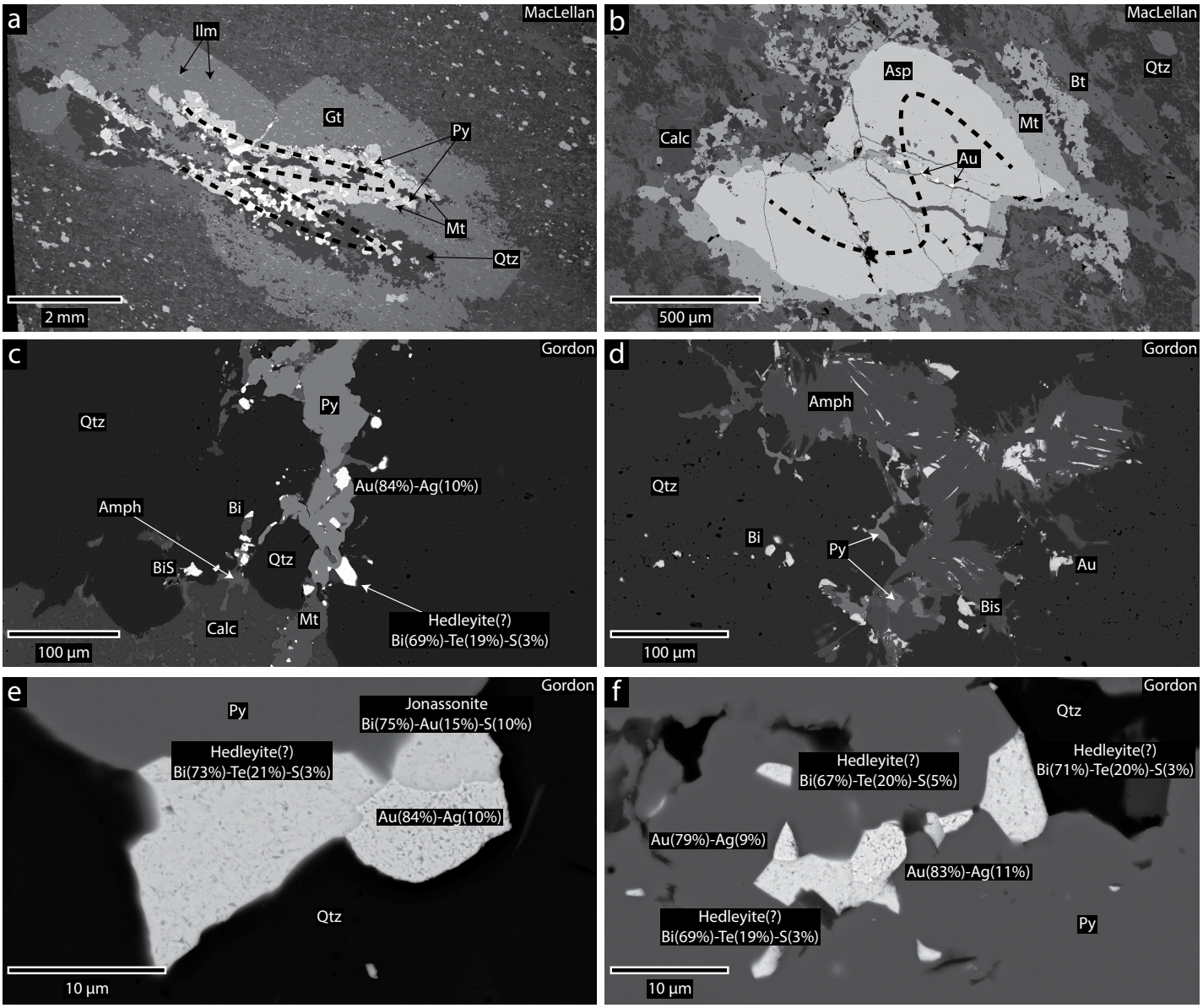

Figure 6

Scanning electron microscope (SEM) backscattered electron (BSE) images of detrital zircons

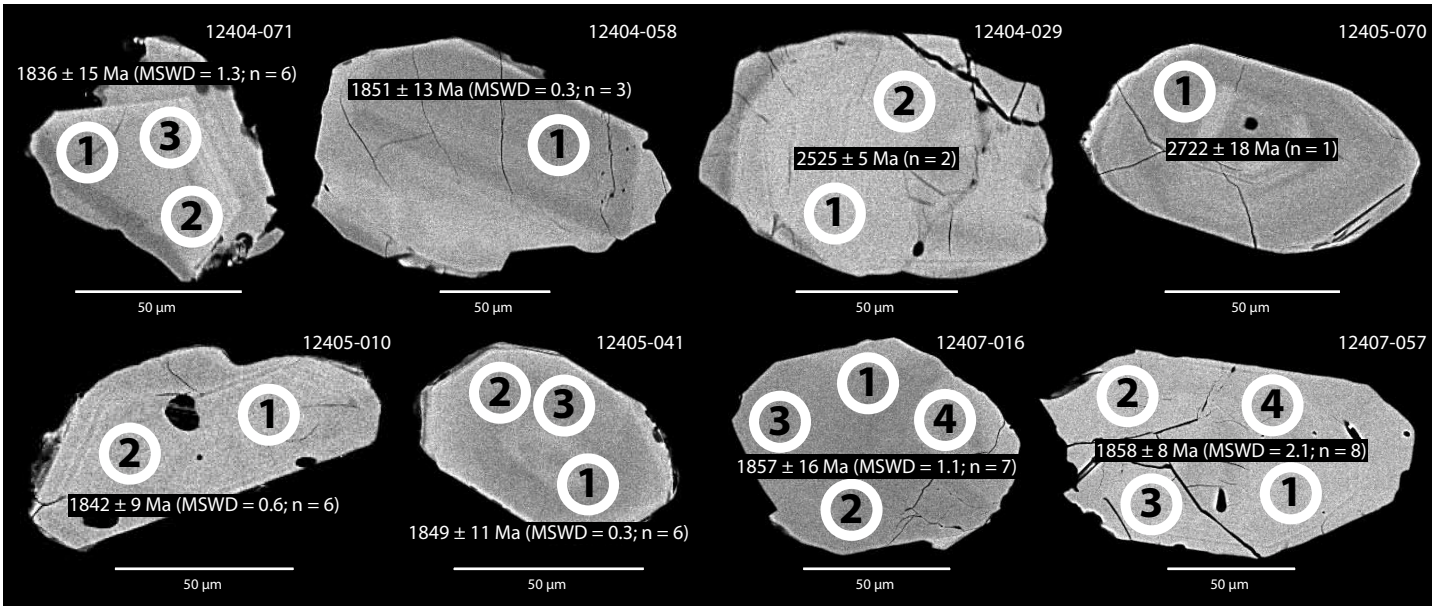

Figure 7

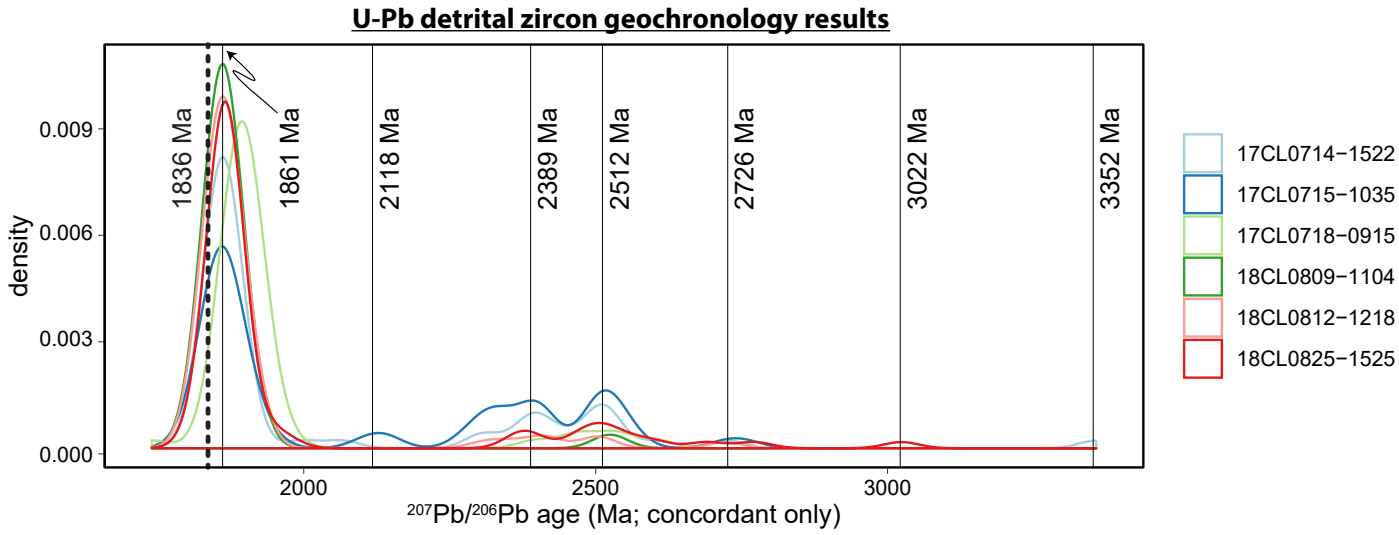
U-Pb detrital zircon geochronology results
1836 Ma
1861 Ma
2118 Ma
2389 Ma
2512 Ma
2726 Ma
3022 Ma
3352 Ma
density
0.009
0.006
0.003
0.000
2000
2500
3000
207Pb/206Pb age (Ma; concordant only)
17CL0714−1522
17CL0715−1035
17CL0718−0915
18CL0809−1104
18CL0812−1218
18CL0825−1525

Figure 8

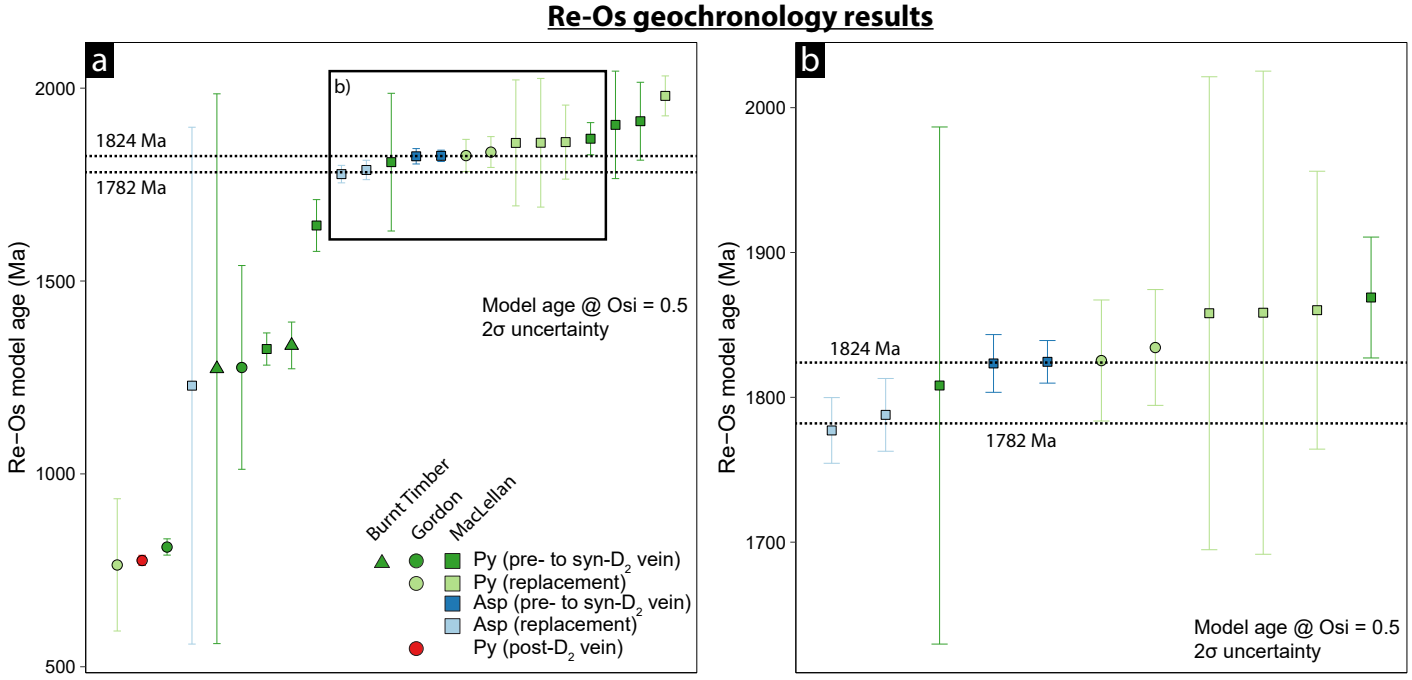
Re-Os geochronology results
a
b)
b
1824 Ma
1782 Ma
Re–Os model age (Ma)
2000
1500
1000
500
1900
1800
1700
Model age @ Osi = 0.5
2σ uncertainty
Burnt Timber
Gordon
MacLellan
Py (pre- to syn-D2 vein)
Py (replacement)
Asp (pre- to syn-D2 vein)
Asp (replacement)
Py (post-D2 vein)

Figure 9

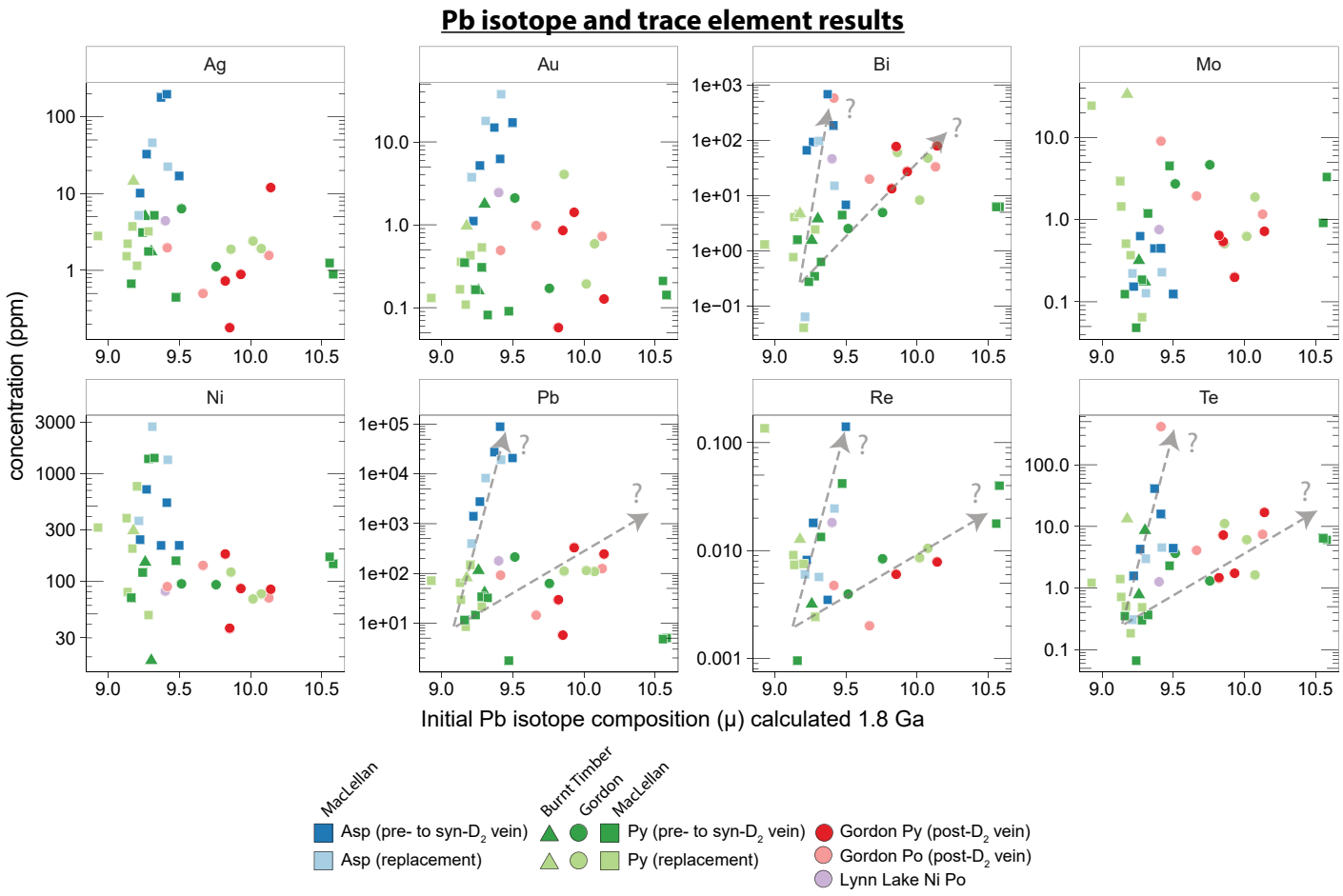
Pb isotope and trace element results
Ag
Au
Bi
Mo
Ni
Pb
Re
Te
concentration (ppm)
Initial Pb isotope composition (μ) calculated 1.8 Ga
MacLellan
Asp (pre- to syn-D2 vein)
Asp (replacement)
Burnt Timber
Gordon
MacLellan
Py (pre- to syn-D2 vein)
Py (replacement)
Gordon Py (post-D2 vein)
Gordon Po (post-D2 vein)
Lynn Lake Ni Po

Figure 10

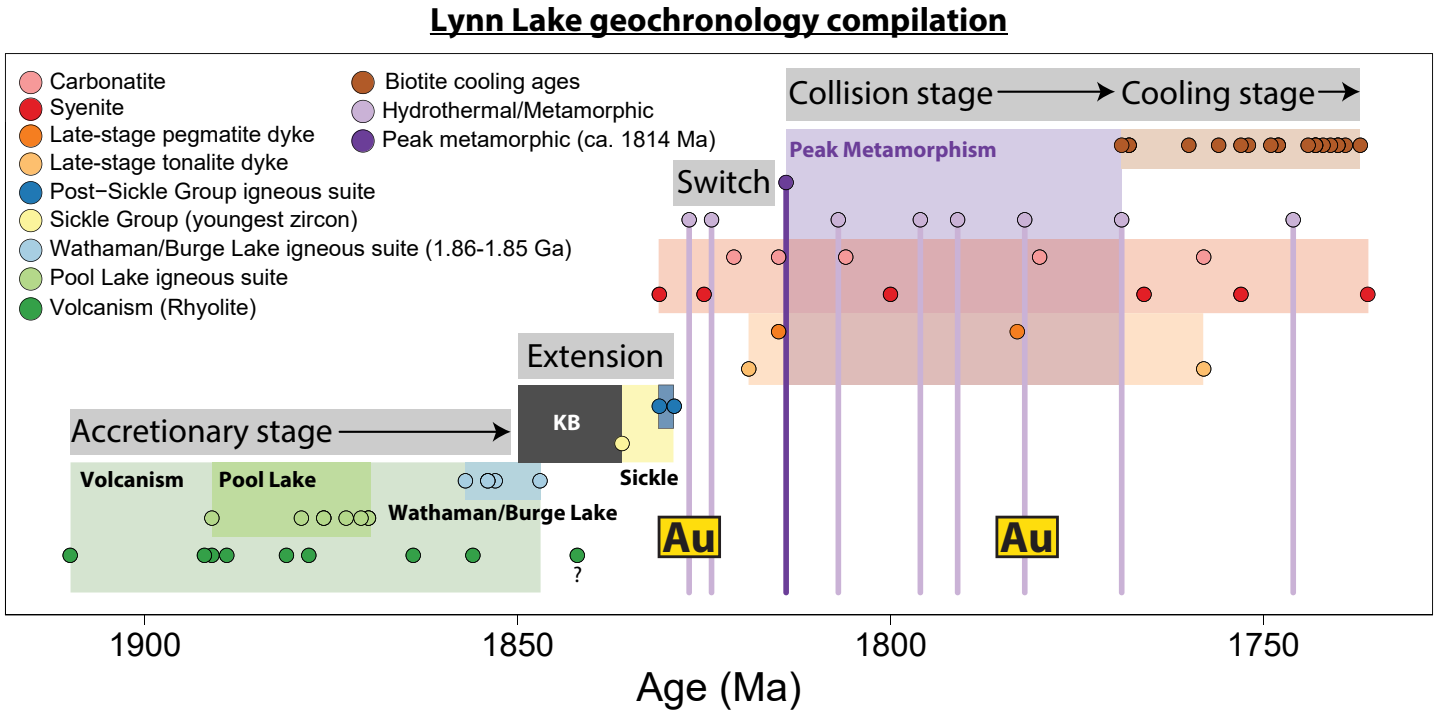
Lynn Lake geochronology compilation
Carbonatite
Syenite
Late-stage pegmatite dyke
Late-stage tonalite dyke
Post−Sickle Group igneous suite
Sickle Group (youngest zircon)
Wathaman/Burge Lake igneous suite (1.86-1.85 Ga)
Pool Lake igneous suite
Volcanism (Rhyolite)
Biotite cooling ages
Hydrothermal/Metamorphic
Peak metamorphic (ca. 1814 Ma)
Collision stage
Cooling stage
Peak Metamorphism
Switch
Extension
Accretionary stage
KB
Sickle
Volcanism
Pool Lake
Wathaman/Burge Lake
?
Au
Au
1900
1850
1800
1750
Age (Ma)

Figure 11

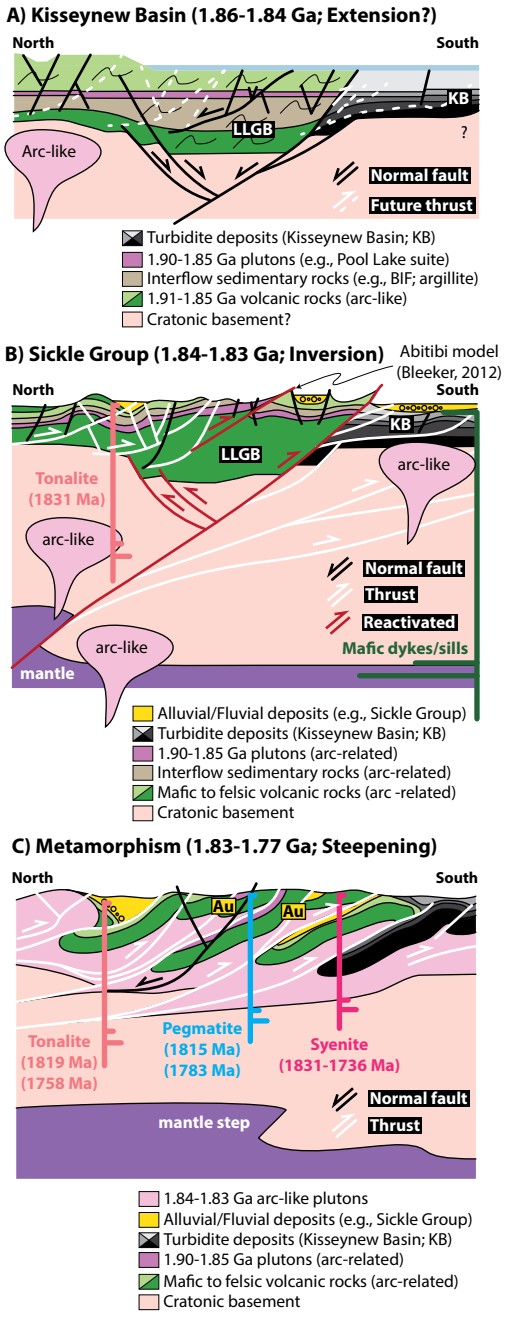
A) Kisseynew Basin (1.86-1.84 Ga; Extension?)
North
South
KB
LLGB
?
Arc-like
Normal fault
Future thrust
Turbidite deposits (Kisseynew Basin; KB)
1.90-1.85 Ga plutons (e.g., Pool Lake suite)
Interflow sedimentary rocks (e.g., BIF; argillite)
1.91-1.85 Ga volcanic rocks (arc-like)
Cratonic basement?
B) Sickle Group (1.84-1.83 Ga; Inversion)
Abitibi model
(Bleeker, 2012)
North
South
KB
LLGB
arc-like
Tonalite
(1831 Ma)
arc-like
Normal fault
Thrust
Reactivated
Mafic dykes/sills
arc-like
mantle
Alluvial/Fluvial deposits (e.g., Sickle Group)
Turbidite deposits (Kisseynew Basin; KB)
1.90-1.85 Ga plutons (arc-related)
Interflow sedimentary rocks (arc-related)
Mafic to felsic volcanic rocks (arc -related)
Cratonic basement
C) Metamorphism (1.83-1.77 Ga; Steepening)
North
South
Au
Au
Tonalite
(1819 Ma)
(1758 Ma)
Pegmatite
(1815 Ma)
(1783 Ma)
Syenite
(1831-1736 Ma)
Normal fault
Thrust
mantle step
1.84-1.83 Ga arc-like plutons
Alluvial/Fluvial deposits (e.g., Sickle Group)
Turbidite deposits (Kisseynew Basin; KB)
1.90-1.85 Ga plutons (arc-related)
Mafic to felsic volcanic rocks (arc-related)
Cratonic basement

Figure 12